

*Constraining Star Formation Histories of Blue Galaxies Using the Scatter between Halo Mass and Stellar Mass*

Star Formation Histories of Star Forming Galaxies in a Hierarchical Universe

CHANGHOON HAHN,<sup>1,2,3,\*</sup> JEREMY L. TINKER,<sup>3</sup> AND ANDREW R. WETZEL<sup>4,5,6</sup>

<sup>1</sup>Lawrence Berkeley National Laboratory, 1 Cyclotron Rd, Berkeley CA 94720, USA

<sup>2</sup>Berkeley Center for Cosmological Physics, University of California, Berkeley, CA 94720, USA

<sup>3</sup>Center for Cosmology and Particle Physics, Department of Physics, New York University, 4 Washington Place, New York, NY 10003

<sup>4</sup>TAPIR, California Institute of Technology, Pasadena, CA USA

<sup>5</sup>Carnegie Observatories, Pasadena, CA USA

<sup>6</sup>Department of Physics, University of California, Davis, CA USA

# ABSTRACT

We present constraints on the timescale of star formation variability and the correlation between star formation and host halo accretion histories of star-forming central galaxies from measurements of the stellar-to-halo mass relation (SHMR). Star-forming galaxies are found to have a tight relationship between their star formation rates and stellar masses on the so-called “star-forming sequence” (SFS), which characterizes both their star formation histories and stellar mass growths. Meanwhile, observed constraints on the SHMR connect stellar mass growth to host halo accretion history. Combining these observed trends with a high-resolution cosmological  $N$ -body simulation, we present flexible models that track the star formation, stellar mass, and host halo accretion histories of star-forming central galaxies over  $z < 1$  while reproducing the observed stellar mass function and SFS of central galaxies in SDSS Data Release 7. Using these models, we find that the scatter in SHMR at  $M_h = 10^{12} M_\odot$ ,  $\sigma_{\log M_*}^{10^{12} M_\odot}$ , is sensitive to the timescale of star formation variability,  $t_{\text{duty}}$ , and the correlation coefficient,  $r$ , between star formation and host halo accretion histories: shorter  $t_{\text{duty}}$  and higher  $r$  both result in tighter  $\sigma_{\log M_*}^{10^{12} M_\odot}$ . To reproduce the constant  $\sigma_{\log M_*} \sim 0.2$  dex over  $z = 1$  to 0 from observed halo model constraints, our model requires  $t_{\text{duty}} \leq 1.5$  Gyr for  $r = 0.99$  or  $r > 0.7$  for  $t_{\text{duty}} = 0.5$  Gyr. For  $r \sim 0.6$ , as found in the literature,  $t_{\text{duty}} < 0.5$  Gyr is necessary. Meanwhile, to reproduce the  $\sigma_{\log M_*}^{10^{12} M_\odot} = 0.35$  to 0.2 dex evolution from  $z = 1$  to 0 in Illustris TNG, our model requires  $t_{\text{duty}} = 0.5$  Gyr for  $r > 0.5$ . Although, the lack of consensus among the SHMRs of observations and galaxy formation models remains the main bottleneck in precisely constraining  $r$  and  $t_{\text{duty}}$ , we demonstrate that SHMR can be used to constrain star formation and host halo accretion histories of SF central galaxies.

*lack of constraints in  $\sigma_{\log M_*}$  at  $10^{12}$  and at  $z = 1$ .*

**Keywords:** methods: numerical – galaxies: evolution – galaxies: haloes – galaxies: star formation – galaxies: groups: general – cosmology: observations.

*This opens* \* hahn.changhoon@gmail.com

*can of worms of: does TNG have these parameters?*

*More SHMR to abundance matching.*

## 1. INTRODUCTION

Observations from large surveys such as the Sloan Digital Sky Survey (SDSS; York et al. 2000) have been critical for establishing the global trends of galaxies in the local universe. Broadly speaking, galaxies fall into two categories: quiescent and star-forming (hereafter SF) galaxies. Quiescent galaxies have little to no star formation, are red in color due to old stellar populations, and have elliptical morphologies. Meanwhile, SF galaxies have significant star formation, thus are blue in color, and have disk-like morphologies (Kauffmann et al. 2003; Blanton et al. 2003; Baldry et al. 2006; Taylor et al. 2009; Moustakas et al. 2013; see Blanton & Moustakas 2009 and references therein). SF galaxies, furthermore, are found on the so-called “star-forming sequence” (hereafter SFS), a tight relationship between their star formation rates (SFR) and stellar masses (Noeske et al. 2007; Daddi et al. 2007; Salim et al. 2007; Speagle et al. 2014; Lee et al. 2015, see also Figure 1). This sequence, which is observed out to  $z > 2$  (Wang et al. 2013; Leja et al. 2015) plays a crucial role in determining galaxy evolution over the past  $\sim 10$  Gyr (see Kelson 2014; Abramson et al. 2016, for an alternative point of view). The significant fraction of SF galaxies that quench their star formation and migrate off of the SFS reflects the growth in the fraction of quiescent galaxies (Blanton 2006; Borch et al. 2006; Bundy et al. 2006; Moustakas et al. 2013). The decline of star formation in the entire SFS (Lee et al. 2015; Schreiber et al. 2015) over time reflects the decline in overall cosmic star formation (Hopkins & Beacom 2006; Behroozi et al. 2013; Madau & Dickinson 2014). With its evolution, the SFS also connects the star formation histories of SF galaxies to their stellar mass growths.

Recent observations have also allowed us to investigate how galaxies fit into the context of hierarchical structure formation predicted by  $\Lambda$ CDM cosmology. In addition to traditional theoretical models of hydrodynamic simulations and semi-analytic models (see Silk & Mamon 2012; Somerville & Davé 2015, for reviews), empirical models have been remarkably effective for understanding the galaxy-halo connection. These models relate galaxy properties to their host dark matter halo properties using methods such as halo occupation distribution modeling (HOD; *e.g.* Zheng et al. 2007; Zehavi et al. 2011; Leauthaud et al. 2012; Parejko et al. 2013; Zu & Mandelbaum 2015), conditional luminosity function modeling (*e.g.* Yang et al. 2009), and abundance matching (*e.g.* Kravtsov et al. 2004; Vale & Ostriker 2006; Conroy et al. 2009; Moster et al. 2013; Reddick et al. 2013). Using these models, we find that more massive halos host more massive galaxies with a tight scatter in the stellar-to-halo mass relation (hereafter SHMR; Mandelbaum et al. 2006; Conroy et al. 2007; More et al. 2011; Leauthaud et al. 2012; Tinker et al. 2013; Velander et al. 2014; Han et al. 2015; Zu & Mandelbaum 2015; Gu et al. 2016; Lange et al. 2018). A similarly tight SHMR is found at higher  $z \sim 1$  (Leauthaud et al. 2012; Tinker et al. 2013; Patel et al. 2015). The tight SHMR over  $z < 1$  suggests that stellar mass growth of galaxies is linked somehow to the growth of their host dark matter halos.

Despite these developments, we face a number of challenges when it comes to understanding the detailed star formation histories (SFH) and its connection to host halo assembly history of galaxies. For instance, SFHs at lookback times longer than 200 Myr do not contribute to SFR indicators such as  $H\alpha$  or  $FUV$  fluxes Sparre et al. (2017). Measuring SFHs from fitting photometry or spectroscopy typically assume a specific functional form of the SFH, such as exponentially declining or lognormal,

define scatter. mention constraints all low, but these driven by higher mass halos.

mention the values

don't say this - say scatter

that do not include variations on short timescales (*e.g.* Wilkinson et al. 2017; Carnall et al. 2018). Even methods that recover non-parametric SFHs from high signal-to-noise observations can only retrieve SFHs in coarse temporal resolutions (*e.g.* Tojeiro et al. 2009; Leja et al. 2018). While simulations provide another means for understanding SFHs, they are also subject to their specific time and mass resolutions that suppress the variability of their star formation, especially in analytic models, semi-analytic models, and large-volume cosmological hydrodynamic simulations (Sparre et al. 2015, 2017, see also Figure 2).

Empirical models, through their flexibility, provide an effective method for examining the connection between SFH and host halo assembly history. A number of empirical models (Taghizadeh-Popp et al. 2015; Becker 2015; Rodríguez-Puebla et al. 2016; Mitra et al. 2017; Cohn 2017; Moster et al. 2017), relate SFHs of galaxies linearly to their host halo mass accretion rates and successfully reproduce a number of observations. Such models make the strong assumption that SFH of galaxies are perfectly correlated to halo accretion history. Recently by analyzing the observed correlation between the SFRs and large-scale environment of SF galaxies, Tinker et al. (2018a) found the first observational evidence that this is true, but with a correlation coefficient of  $r \sim 0.63$ . These models, therefore, ignore variation in star formation independent from halo accretion, which may come from physical processes in galaxies. More recently, the empirical model of Behroozi et al. (2018) <sup>update</sup> correlate SFH with halo assembly while also incorporating star formation variability in the SFH. For halos at a given  $v_{\text{Mpeak}}$  (the maximum circular velocity of the halo at the redshift of max halo mass) and  $z$ , they assign higher SFRs to halos with higher values of  $\Delta v_{\text{max}}$  (logarithmic growth in the maximum circular velocity of the halo over past dynamical time) allowing for random scatter in the assignment. Through this random scatter, which is further separated into contributions from shorter and longer timescales, they incorporate star formation variability. Explicitly examining and constraining the timescale of star formation variability, however, is difficult with such a parameterization. Such constraints can shed light on physical processes involved in galaxy star formation and constrain galaxy feedback models (Sparre et al. 2015). For instance, it can be used to differentiate between physical processes such as galactic feedback interacting with the circumgalactic medium, which would cause longer timescale variations, or internal processes affecting the cold gas in the galaxy, which would cause  $\sim 100$  Myr variations. Using the Feedback In Realistic Environments (FIRE) high resolution cosmological simulations, Hopkins et al. (2014) find that explicit and resolved feedback increases time variability in SFRs. Also using FIRE, Sparre et al. (2017) find that varying the strength of Type II supernova feedback can change the burstiness of SFHs. Governato et al. (2015) find that HI shielding from UV radiation and early feedback from young stars would also produce small scale star formation variability.

In this paper, we construct empirical models to investigate the timescale of star formation variability and the connection between SFH and host halo accretion history of SF central galaxies. Central galaxies constitute the majority of massive galaxies ( $M_* > 10^{9.5} M_\odot$ ) at  $z \sim 0$  (Wetzel et al. 2013) and their SFHs are not influenced by environmentally-driven external mechanisms, such as ram pressure stripping (Gunn & Gott 1972; Bekki 2009), strangulation (Larson et al. 1980; Peng et al. 2015), or harassment (Moore et al. 1998) (that impact SFHs of satellites). Using a similar approach as Wetzel

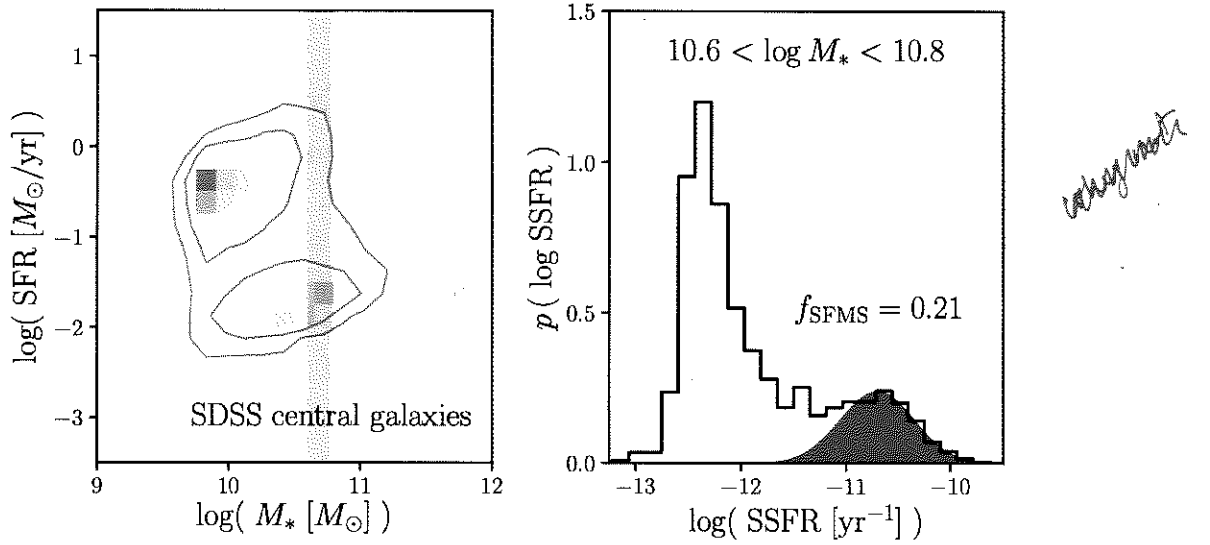


**Figure 1.** The SFR- $M_*$  relation of the central galaxies in SDSS DR7 mark the bimodal distribution of the SF and quiescent populations (left panel). *SF centrals, based on the correlation between their SFR and  $M_*$ , lie on the so-called “star-forming sequence”.* On the right, we present the SSFR distribution,  $p(\log \text{SSFR})$ , of SDSS centrals with  $10.6 < \log M_* < 10.8$ . Based on the SFS component from the Hahn et al. (2018b) GMM fit to the SFR- $M_*$  relation (shaded in blue), galaxies in the SFS account for  $f_{\text{SFS}} = 0.21$  of the centrals in the stellar mass bin.

et al. (2013); Hahn et al. (2017a), we present models that combine a high resolution cosmological  $N$ -body simulation with observed evolutionary trends of the SFS. They statistically track the star formation, stellar mass, and host halo assembly histories of SF central galaxies from  $z \sim 1$  to 0. After fitting our models to reproduce the properties of observed SF central galaxies, we compare the predicted SHMR, in particular the scatter in the SHMR  $\sigma_{\log M_*}$  at  $M_h = 10^{12} M_\odot$  (hereafter  $\sigma_{\log M_*}^{10^{12} M_\odot}$ ), of our model to constraints from observations and modern galaxy formation models. This comparison allows us to constrain the timescale of star formation variability and the correlation between SFH and host halo assembly history. We focus on constraints derived from a constant  $\sigma_{\log M_*} \sim 0.2$  dex from  $z = 1$  to 0 as found in halo model analyses. These analyses, however, mainly constrain  $\sigma_{\log M_*}$  at  $M_h > 10^{12} M_\odot$ . In the recent Cao et al. (in preparation) analysis, they find larger  $\sigma_{\log M_*}^{10^{12} M_\odot} \sim 0.3$  dex from observations. They also find that in the Illustris TNG (Pillepich et al. 2018) hydrodynamic simulation,  $\sigma_{\log M_*}^{10^{12} M_\odot}$  decreases from  $z = 1$  to 0. We, therefore, also focus on constraints for a scenario  $\sigma_{\log M_*}$  that decreases over cosmic time. In Section 2 we describe the  $z \approx 0$  central galaxy sample used to compare our models that we construct from SDSS Data Release 7. Then in Section 3, we describe the  $N$ -body simulation and how we evolve the SFR and stellar masses of the SF central galaxies in our model. We compare predictions from our model to observations and present the resulting constraints in Section 4. Finally, we conclude and summarize the results in Section 5.

- What is required to keep  $\sigma$  constant?
- What is required to reduce  $\sigma$ ?
- How change when  $\sigma(z=1)$  change?

## 2. CENTRAL GALAXIES OF SDSS DR7

→ These are the questions we will answer.

We will consider multiple scenarios, with constant or decreasing  $\sigma$  as our fiducial model.

↓  
single  
already  
published

We construct our galaxy sample following the sample selection of Tinker et al. (2011). We select a volume-limited sample of galaxies at  $z \approx 0.04$  with  $M_r - 5\log(h) < -18$  and complete above  $M_* > 10^{9.4}h^{-2}M_\odot$  from the NYU Value-Added Galaxy Catalog (VAGC; Blanton et al. 2005) of the Sloan Digital Sky Survey Data Release 7 (SDSS DR7; Abazajian et al. 2009). The stellar masses of these galaxies are estimated using the `kcorrect` code (Blanton & Roweis 2007) assuming a Chabrier (2003) initial mass function. For their specific star formation rates (SSFR) we use measurements from the current release of the MPA-JHU spectral reductions<sup>1</sup> (Brinchmann et al. 2004). Generally,  $\text{SSFR} > 10^{-11}\text{yr}^{-1}$  are derived from  $\text{H}\alpha$  emission,  $10^{-11} > \text{SSFR} > 10^{-12}\text{yr}^{-1}$  are derived from a combination of emission lines, and  $\text{SSFR} < 10^{-12}\text{yr}^{-1}$  are based on  $D_n4000$  (see discussion in Wetzel et al. 2013). We emphasize that  $\text{SSFR} < 10^{-12}\text{yr}^{-1}$  should only be considered upper limits to the actual galaxy SSFR (Salim et al. 2007).

From this galaxy sample, we identify central galaxies using the Tinker et al. (2011) group finder, a halo-based algorithm that uses the abundance matching ansatz to iteratively assign halo masses to groups (see also Yang et al. 2005). [It assigns an initial halo mass to each galaxy by matching their abundances. Then starting with the most massive galaxy, nearby lower mass galaxies are assigned a probability of being a satellite. Once all the galaxies are assigned to a group, the halo masses of the central galaxies are updated by abundance matching with the total stellar mass in the groups. This entire process is repeated until convergence.] Every group contains one central galaxy, which by definition is the most massive, and a group can contain zero, one, or many satellites. As with any group finder, galaxies are misassigned due to projection effects and redshift space distortions. Our central galaxy sample has a purity of  $\sim 90\%$  and completeness of  $\sim 95\%$  (Tinker et al. 2018b). Moreover, as illustrated in Campbell et al. (2015), the Tinker et al. (2011) group finder robustly identifies red and blue centrals as a function of stellar mass, which is highly relevant to our analysis. We present the  $\text{SFR}-M_*$  relation of the SDSS DR7 central galaxies, described above, in the left panel of Figure 1. The contours of the relation clearly illustrate the bimodality in the galaxy sample with the star-forming centrals lying on the so-call “star-forming sequence” (SFS).

### 3. MODEL: SIMULATED CENTRAL GALAXIES

We are interesting in constructing a model that tracks central galaxies and their star formation within the heirarchical growth of their host halos. This requires a cosmological  $N$ -body simulation that accounts for the complex dynamical processes that govern the host halos of galaxies. In this paper we use the high resolution  $N$ -body simulation from Wetzel et al. (2013) generated using the White (2002) `TreePM` code with flat  $\Lambda$ CDM cosmology ( $\Omega_m = 0.274$ ,  $\Omega_b = 0.0457$ ,  $h = 0.7$ ,  $n = 0.95$ , and  $\sigma_8 = 0.8$ ). From initial conditions at  $z = 150$ , generated from second-order Lagrangian Perturbation Theory,  $2048^3$  particles with mass of  $1.98 \times 10^8 M_\odot$  are evolved in a  $250 h^{-1}\text{Mpc}$  box with a Plummer equivalent smoothing of  $2.5 h^{-1}\text{kpc}$  (Wetzel et al. 2013, 2014). ‘Host halos’ are then identified using the Friends-of-Friends algorithm (FoF; Davis et al. 1985) with linking length of  $b=0.168$  times the mean inter-partcile spacing. Within these host halos, Wetzel et al. (2013) identifies ‘subhalos’ as overdensities in phase space through a six-dimensional FoF algorithm (FoF6D; White et al. 2010).

<sup>1</sup> <http://wwwmpa.mpa-garching.mpg.de/SDSS/DR7/>

The host halos and subhalos are then tracked across the simulation outputs from  $z = 10$  to 0 to build merger trees (Wetzel et al. 2009; Wetzel & White 2010). The most massive subhalos in newly-formed host halos at a given simulation output are defined as the ‘central’ subhalo. A central subhalo retains its ‘central’ definition until it falls into a more massive host halo (FoF halo mass), at which point it becomes a ‘satellite’ subhalo.

Throughout its 45 snapshot outputs, **TreePM** simulation tracks the evolution of subhalos back to  $z \sim 10$ . We restrict ourselves to 15 snapshots from  $z = 1.08$  to 0.05, where we have the most statistically meaningful observations. Furthermore, since we are interested in centrals we only keep subhalos that are classified as centrals throughout the redshift range. This criterion removes “black splash” or “ejected” satellite galaxies (*e.g.* Mamon et al. 2004; Wetzel et al. 2014) misclassified as centrals. Next, we describe how we select and initialize the SF central galaxies from the central subhalos of the **TreePM** simulation in our model.

### 3.1. Selecting Star-Forming Centrals

To construct a model that tracks the SFR and stellar mass evolution of star-forming central galaxies, we first need to select them from the central galaxies/subhalos in the **TreePM** simulation. Since we want our model to reproduce observations, our selection is based on  $f_{\text{SFS}}^{\text{cen}}(M_*)$ , the fraction of central galaxies within the SFS measured from the SDSS DR7 VAGC (Section 2). Below, we describe how we derive  $f_{\text{SFS}}^{\text{cen}}(M_*)$  and use it to select SF central galaxies in our model. Afterwards we describe how we initialize the SFRs and  $M_*$  of these galaxies at  $z = 1$ .

Often in the literature, an empirical color-color or SFR- $M_*$  cut that separates the two main modes (red/blue or star-forming/quiescent) in the distribution is chosen to classify galaxies (*e.g.* Baldry et al. 2006; Blanton & Moustakas 2009; Drory et al. 2009; Peng et al. 2010; Moustakas et al. 2013; Hahn et al. 2015). The red/quiescent or blue/star-forming fractions derived from this sort of classification, by construction, depend on the choice of cut and neglect galaxy subpopulations such as transitioning galaxies *i.e.* galaxies in the “green valley”. Instead, for our  $f_{\text{SFS}}^{\text{cen}}(M_*)$ , we use the SFS identified from the Hahn et al. (2018b) method, which uses Gaussian Mixture Models and the Bayesian Information Criteria to fit the SFR- $M_*$  relation of a galaxy population and identify its SFS. This data-driven approach relaxes many of the assumptions and hard cuts that go into other methods and can be flexibly applied to a wide range of SFRs and  $M_*$ s and for multiple simulations. The weight of the SFS GMM component from the method provides an estimate of  $f_{\text{SFS}}^{\text{cen}}$ . In the right panel of Figure 1, we present the SSFR distribution,  $p(\log \text{SSFR})$ , of the SDSS DR7 central galaxies within  $10.6 < \log M_* < 10.8$  with the SFS GMM component shaded in blue. The SFS constitutes  $f_{\text{SFS}}^{\text{cen}} = 0.21$  of the SDSS central galaxies in this stellar mass bin. Using the  $f_{\text{SFS}}^{\text{cen}}$  estimates, we fit  $f_{\text{SFS}}^{\text{cen}}$  as a linear function of  $\log M_*$  similar to Wetzel et al. (2013); Hahn et al. (2017a):

$$f_{\text{SFS,bestfit}}^{\text{cen}}(M_*) = -0.627 (\log M_* - 10.5) + 0.354. \quad (1)$$

We note that this is in good agreement with the  $f_{\text{Q}}^{\text{cen}}(M_*; z \sim 0)$  fit from Hahn et al. (2017a).

To select the SF centrals from the subhalos, we begin by assigning  $M_*$  at  $z \sim 0$  to the subhalos by subhalo abundance matching (SHAM) to  $M_{\text{peak}}$ , the maximum host halo mass that it ever had as

a central subhalo (Conroy et al. 2006; Vale & Ostriker 2006; Yang et al. 2009; Wetzel et al. 2012; Leja et al. 2013; Wetzel et al. 2013, 2014; Hahn et al. 2017a). SHAM, in its simplest form, assumes a one-to-one mapping between subhalo  $M_{\text{peak}}$  and galaxy stellar mass,  $M_*$ , that preserves rank order:  $n(>M_{\text{peak}}) > n(>M_*)$ . In practice, we apply a 0.2 dex log-normal scatter in  $M_*$  at fixed  $M_{\text{peak}}$  based on the observed SHMR (*e.g.* Mandelbaum et al. 2006; More et al. 2011; Velander et al. 2014; Zu & Mandelbaum 2015; Gu et al. 2016; Lange et al. 2018). For  $n(>M_*)$ , we use observed stellar mass function (SMF) from Li & White (2009), which is based on the same SDSS NYU-VAGC sample as our group catalog. Then using the SHAM  $M_*$ , we randomly select subhalos as SF based on the probabilities of being on the SFS using Eq. 1. Tinker et al. (2017a, 2018b) found that quenching is independent of halo growth rate and therefore we randomly select SF subhalos. In our model, we assume that once a SF galaxy quenches its star formation, it remains quiescent. Without any quiescent galaxies rejuvenating their star formation, galaxies on the SFS at  $z \sim 0$  are also on the SFS at  $z > 0$ . Using this assumption the SF centrals we select at  $z \sim 0$  are also on the SFS at the initial redshift of our model:  $z \sim 1$ .

We next initialize the SF centrals at  $z \sim 1$  using the observed SFR- $M_*$  relation of the SFS with  $M_*$  assigned using SHAM with a  $z \sim 1$  SMF interpolated between the Li & White (2009) SMF and the SMF from Marcesini et al. (2009) at  $z = 1.6$ . We choose the Marcesini et al. (2009) SMF, among others, because it produces interpolated SMFs that monotonically increase over  $z < 1$ . As noted in Hahn et al. (2017a), at  $z \approx 1$ , the SMF interpolated between the Li & White (2009) and Marcesini et al. (2009) SMFs is consistent with more recent measurements from Muzzin et al. (2013) and Ilbert et al. (2013). We apply a  $\sigma_{\log M_*}^{\text{init}} = 0.2$  dex log-normal scatter in the SHAM based on observations (*e.g.* Leauthaud et al. 2012; Tinker et al. 2013; Patel et al. 2015). We next assign SFRs based on  $z \sim 1$  observations in the literature. However, observations, not only use galaxy properties derived differently from the SDSS VAGC but they also find SFS with significant discrepancies from one another. In a compilation of SFSs from 25 studies in the literature, Speagle et al. (2014) find that the SFRs of the SFSs at  $z \sim 1$  vary by more than a factor of 2 at  $M_* = 10^{10.5} M_\odot$ , even after their calibration (see Figure 2 of Speagle et al. 2014). With little consensus on the SFS at  $z \sim 1$ , and consequently its redshift evolution, we flexibly parameterize the SFS SFR,  $\log \text{SFR}_{\text{SFS}}(M_*, z)$ , with free parameters that characterize the stellar mass dependence of the SFS below and above  $10^{10} M_\odot$  and the redshift dependence ( $m_{M_*}^{\text{low}}$ ,  $m_{M_*}^{\text{high}}$ , and  $m_z$ , respectively):

$$\log \text{SFR}_{\text{SFS}}(M_*, z) = m_{M_*} (\log M_* - 10.) + m_z (z - 0.05) - 0.19 \quad (2)$$

$$\text{where } m_{M_*} = \begin{cases} m_{M_*}^{\text{low}} & \text{for } M_* < 10^{10} M_\odot \\ m_{M_*}^{\text{high}} & \text{for } M_* \geq 10^{10} M_\odot. \end{cases}$$

We assign SFRs to our SF centrals at  $z \sim 1$  by sampling a log-normal distribution centered about  $\log \text{SFR}_{\text{SFS}}(M_*, z = 1)$  with a constant scatter of 0.3 dex from observations (Daddi et al. 2007; Noeske et al. 2007; Magdis et al. 2012; Whitaker et al. 2012). Later when comparing to observations, we choose conservative priors for the parameters  $m_{M_*}^{\text{low}}$ ,  $m_{M_*}^{\text{high}}$  and  $m_z$  that encompass the best-fit SFS from Speagle et al. (2014) as well as measurements from Moustakas et al. (2013) and Lee et al. (2015). With our SF centrals initialized at  $z \sim 1$ , next, we describe how we evolve their SFR and  $M_*$ .

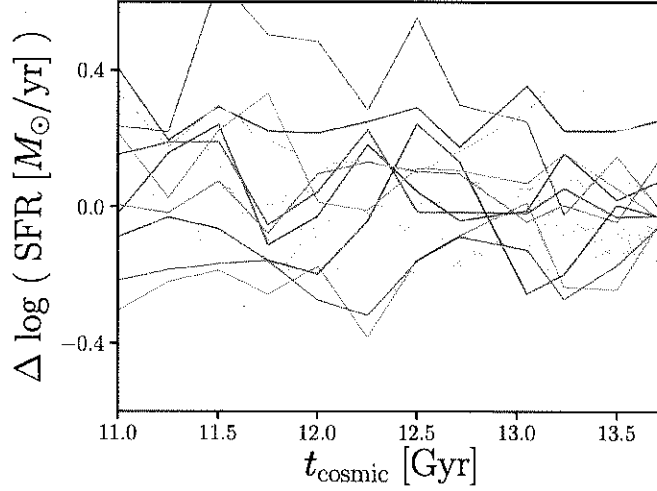


**Figure 2.** Galaxies in the Illustris hydrodynamical simulation have SFHs that evolve along the SFS, with their SFRs stochastically fluctuating about the mean log SFR of the SFS. We highlight  $\Delta \log \text{SFR}$ , SFR with respect to  $\log \text{SFR}_{\text{SFS}}$  (Eq. 3), for a handful of galaxies with  $10^{10.5} < M_* < 10^{10.6} M_\odot$  at  $z \sim 0$ . We calculate  $\Delta \log \text{SFR}$  with  $\log \text{SFR}_{\text{SFS}}$  identified using the Hahn et al. (2018b) method, same as in Section 3.1. The implementation of SFR variability in the SFHs of SF centrals in our model (Section 3.2) is motivated by the SFHs of Illustris galaxies above.

### 3.2. Evolving along the Star Formation Sequence

The tight correlation between the SFRs and  $M_*$  of SF galaxies on the SFS has been observed spanning over four orders of magnitude in stellar mass, with a roughly constant scatter of  $\sim 0.3$  dex, and out to  $z > 2$  (e.g. Noeske et al. 2007; Daddi et al. 2007; Elbaz et al. 2007; Salim et al. 2007; Santini et al. 2009; Karim et al. 2011; Whitaker et al. 2012; Moustakas et al. 2013; Lee et al. 2015; see also references in Speagle et al. 2014). This correlation is also predicted by modern galaxy formation models (Somerville & Davé 2015, see Hahn et al. 2018b and references therein). The SFS naturally presents itself as an anchoring relationship to characterize the star formation and  $M_*$  growth histories of SF galaxies throughout  $z < 1$ . We, therefore, characterize the SFH of each star-forming central with respect to the  $\log \text{SFR}$  of the SFS (Eq. 2):

$$\log \text{SFR}_i(M_*, t) = \log \text{SFR}_{\text{SFS}}(M_*, t) + \Delta \log \text{SFR}_i(t). \quad (3)$$

Since SFHs determine the  $M_*$  growth of galaxies, in this prescription,  $\Delta \log \text{SFR}_i(t)$  dictates the SFH and  $M_*$  evolution of SF central.

One simple prescription for  $\Delta \log \text{SFR}(t)$  would be to keep  $\Delta \log \text{SFR}$  fixed throughout  $z < 1$  to the offsets from the  $\log \text{SFR}_{\text{SFS}}$  in the initial SFRs of our SF centrals at  $z \sim 1$  similar to simple analytic models such as Mitra et al. (2015). Galaxies with higher than average initial SFRs continue evolving above the average SFS, while SF centrals with lower than average initial SFRs continue evolving below the average SFS. In addition to not being able to reproduce observations, which we later demonstrate, we also do not find such SFHs in SF galaxies of hydrodynamic simulations such as Illustris (Vogelsberger et al. 2014; Genel et al. 2014). In Figure 2, we plot  $\Delta \log \text{SFR}_i$  of



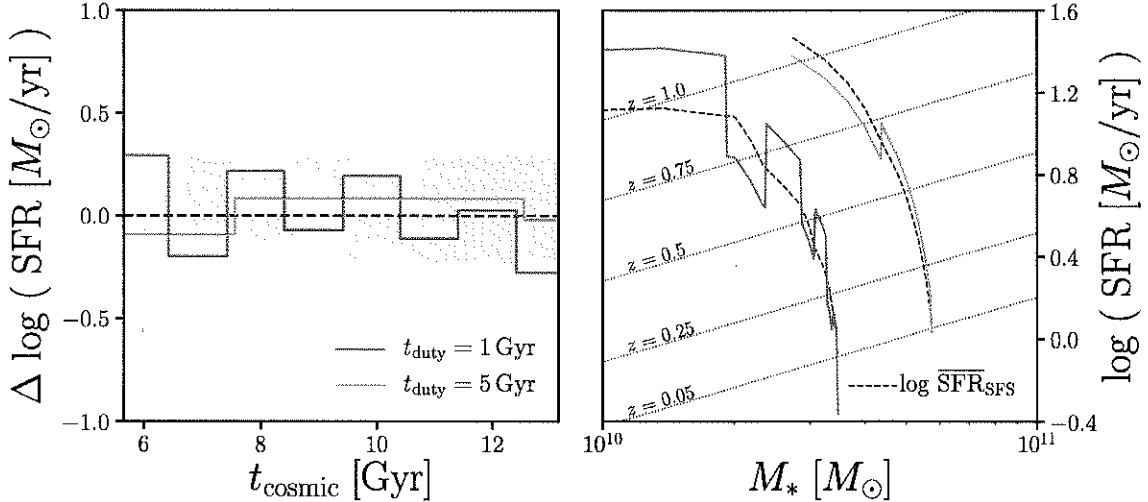


**Figure 3.** We incorporate star formation variability in our model using a “star formation duty cycle” where the SFRs of SF centrals fluctuate about  $\log \text{SFR}_{\text{SFS}}$  on some timescale  $t_{\text{duty}}$ . In our fiducial prescription, we randomly sample  $\Delta \log \text{SFR}$  from a log-normal distribution with 0.3 dex scatter at each duty cycle timestep. We illustrate  $\Delta \log \text{SFR}_i(t)$  of two SF centrals with star formation duty cycles on  $t_{\text{duty}} = 1 \text{ Gyr}$  (blue) and 5 Gyr (orange) timescales in the left panel.  $\Delta \log \text{SFR}(t)$  determines the SFH and hence the  $M_{*}$  growth of the SF central galaxies (Eq. 4). On the right, we illustrate the SFR and  $M_{*}$  evolutions of the corresponding SF centrals. For reference, we include  $\log \text{SFR}_{\text{SFS}}(M_{*,i}(t), t)$  that the galaxies’ SFR and  $M_{*}$  evolve along (black solid). We also include  $\log \text{SFR}_{\text{SFS}}(M_{*})$  at various redshifts between  $z = 1$  to 0.05 (dotted lines). *The SF centrals in our model evolve their SFRs and  $M_{*}$  along the SFS with their SFRs fluctuate about  $\log \text{SFR}_{\text{SFS}}$ .*

star-forming galaxies in the Illustris simulation as a function of cosmic time. These galaxies have  $10^{10.5} M_{\odot} < M_{*} < 10^{10.6} M_{\odot}$  at  $z = 0$ . At each simulation output, we calculate  $\Delta \log \text{SFR}_i$  using Eq. 3 with  $\log \text{SFR}_{\text{SFS}}$  derived from the SFS identified in the simulation using the Hahn et al. (2018b) method, same as in Section 3.1. As the highlighted  $\Delta \log \text{SFR}_i$  illustrate, SF galaxies in Illustris evolve along the SFS, with their SFRs fluctuating about  $\log \text{SFR}_{\text{SFS}}$ .

Motivated by the SFHs of Illustris SF galaxies, we introduce variability to the SFHs of our SF centrals in the form of a “star formation duty cycle”. Within the SFH of Eq. 3, we parameterize  $\Delta \log \text{SFR}_i$  to fluctuate about the  $\log \text{SFR}_{\text{SFS}}$  on timescale,  $t_{\text{duty}}$ , with amplitude sampled from a log-normal distribution with 0.3 dex scatter. For our fiducial star formation duty cycle prescription, we randomly sample  $\Delta \log \text{SFR}_i$  from a log-normal distribution with 0.3 dex scatter. We illustrate  $\Delta \log \text{SFR}_i(t)$  of SF centrals with our star formation duty cycle prescription on  $t_{\text{duty}} = 1 \text{ Gyr}$  (blue) and 5 Gyr (orange) timescales in the left panel of Figure 3. The shaded region represents the observed 0.3 dex scatter of  $\log \text{SFR}$  in the SFS. This  $\Delta \log \text{SFR}$  prescription by construction reproduces the observed log-normal SFR distribution of the SFS at any point in the model. Although, this simplified prescription does not reflect the individual SFHs of SF centrals, we seek to statistically capture the stochasticity from gas accretion, star-bursts, and feedback mechanisms for the entire SF population. Measuring  $t_{\text{duty}}$  in the duty cycle parameterization provides us with an estimate of the timescale

of such star formation variabilities and thus provide a useful constraint on the physics of galaxy formation.

Using our fiducial SFH prescription, we evolve both the SFR and  $M_*$  of our SF centrals along the SFS. Based on Eq. 3, the SFRs of our SF centrals are functions of  $M_*$ , while  $M_*$  is the integral of the SFR over time:

$$M_*(t) = f_{\text{retain}} \int_{t_0}^t \text{SFR}(M_*, t') dt' + M_0. \quad (4)$$

$t_0$  and  $M_0$  are the initial cosmic time and stellar mass at  $z \sim 1$ , respectively.  $f_{\text{retain}}$  here is the fraction of stellar mass that is retained after supernovae and stellar winds; we use  $f_{\text{retain}} = 0.6$  (Wetzel et al. 2013). We can now evolve the SFR and  $M_*$  of our SF centrals until the final  $z = 0.05$  snapshot by solving the differential equation of Eqs. 3 and 4. On the right panel of Figure 3, we present the SFR and  $M_*$  evolutions of two SF centrals with  $t_{\text{duty}} = 1$  Gyr (blue) and 5 Gyr (orange), same as the left panel. For reference, we include the mean log SFR of the SFS that the galaxies' SFR and  $M_*$  evolve along,  $\log \text{SFR}_{\text{SFS}}(M_{*,i}(t), t)$  (black solid). We also include  $\log \text{SFR}_{\text{SFS}}(M_*)$  (dotted lines) at various redshifts between  $z = 1$  to 0.05. Based on the SFH prescription in our model, SF centrals evolve their SFRs and  $M_*$  along the SFS with their SFRs fluctuate about  $\log \text{SFR}_{\text{SFS}}$ .

### 3.3. Adding Assembly Bias *Correlating SFR with halo growth*

In our fiducial SFH prescription, we sample  $\Delta \log \text{SFR}_i$  randomly from a log-normal distribution with 0.3 dex scatter. There is, however, growing evidence that star formation in galaxies correlate with their host halo accretion histories (*e.g.* Lim et al. 2016; Tojeiro et al. 2017; Tinker et al. 2018a). In this section, we introduce *assembly bias* into the SFH prescription of our model. Assembly bias, most commonly in the literature, refers to the dependence of the spatial distribution of dark matter halos on halo properties besides mass (Gao et al. 2005; Wechsler et al. 2006; Gao & White 2007; Wetzel et al. 2007; Li et al. 2008; Sunayama et al. 2016). At low halo mass, older and more concentrated halos form in high density environments. While at high halo mass, the effect is the opposite — younger, less concentrated halos form in high-density regions. However, both simulations (Croton et al. 2007; Artale et al. 2018; Zehavi et al. 2018) as well as observations (Yang et al. 2006; Wang et al. 2008; Tinker et al. 2011; Wang et al. 2013; Lacerna et al. 2014; Calderon et al. 2018; Tinker et al. 2018b), find that this assembly bias propagates beyond spatial clustering and correlates with certain galaxy properties such as formation histories and star formation properties, an effect more specifically referred to as *galaxy assembly bias*. In our model, we incorporate galaxy assembly bias by correlating the SFHs of our SF central galaxies and their host halo accretion histories with a correlation coefficient  $r$ .

We correlate  $\Delta \log \text{SFR}$  (Eq. 3) to the halo mass accretion over dynamical time. At every  $t_{\text{duty}}$  timestep,  $t$ ,  $\Delta \log \text{SFR}(t)$  is assigned based on  $\Delta M_h(t) = M_h(t) - M_h(t - t_{\text{dyn}})$  in  $M_{\text{max}}$  bins with a correlation coefficient  $r$ , a parameter added to our model. This prescription for correlating  $\Delta \log \text{SFR}$  to  $\Delta M_h$  is similar to other empirical models that also correlate  $\Delta \log \text{SFR}$  to  $\Delta M_h$  over  $t_{\text{dyn}}$  (Rodríguez-Puebla et al. 2016; Behroozi et al. 2018). In Rodríguez-Puebla et al. (2016), however, they assume perfect ( $r = 1$ ) correlation between SFH and halo accretion. In the Behroozi et al. (2018) UNI-

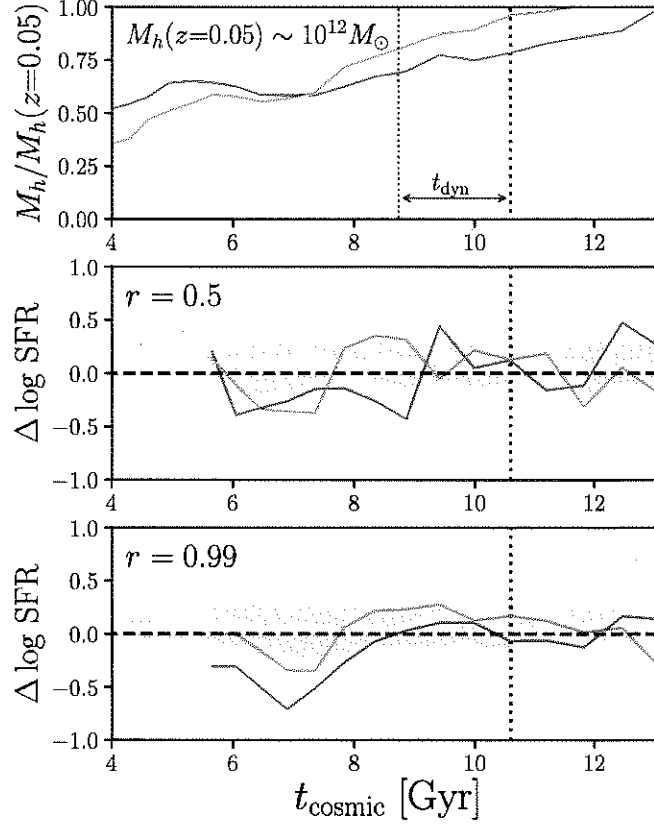


**Figure 4.** We incorporate galaxy assembly bias into the SF centrals of our model by correlating their host halo accretion history with  $\Delta \log \text{SFR}(t)$ , the SFH with respect to the SFS, with correlation coefficient  $r$ . We plot the relative halo accretion history,  $M_h(t)/M_h(z=0.05)$  for two randomly chosen SF centrals with  $M_h(z=0.05) \sim 10^{12} M_\odot$ , in the top panel. In the two panels below we present  $\Delta \log \text{SFR}$ , of these galaxies for our model with  $r = 0.5$  and  $0.99$  (middle and bottom). The shaded region in these panels mark the 0.3 dex 1-sigma width of the log-normal SFS. At some  $t$  (dotted),  $\Delta \log \text{SFR}(t)$  is correlated with halo accretion over the period  $t - t_{\text{dyn}}$  to  $t_{\text{dyn}}$  labeled in top panel. The SFHs illustrate how  $\Delta \log \text{SFR}(t)$  correlates with  $\Delta M_h = M_h(t) - M_h(t - t_{\text{dyn}})$  and how  $\Delta \log \text{SFR}(t)$  correlates more strongly with  $\Delta M_h(t)$  with higher  $r$ .

VERSEMACHINE (hereafter UM),  $r$  is free parameter and their SFH includes SF variability, similar to our model. As we mention in the introduction, their prescription, however, does not focus on a star formation variation on specific timescales, which our models do through the star formation duty cycle.

In Figure 4, we illustrate our prescription for galaxy assembly bias in our model. We plot the relative halo accretion histories  $M_h(t)/M_h(z=0.05)$  of two arbitrarily chosen SF centrals with  $M_h(z=0.05) \sim 10^{12} M_\odot$  in the top panel (orange and blue). Below, we plot  $\Delta \log \text{SFR}$ , SFH with respect to the SFS, of these galaxies for our model with correlation coefficients  $r = 0.5$  and  $0.99$  (middle and bottom). We choose a random TreePM snapshot,  $t$  (dotted), and label the period  $[t, t - t_{\text{dyn}}]$ . Halo accretion over this period,  $\Delta M_h = M_h(t) - M_h(t - t_{\text{dyn}})$ , correlates with  $\Delta \log \text{SFR}(t)$ .

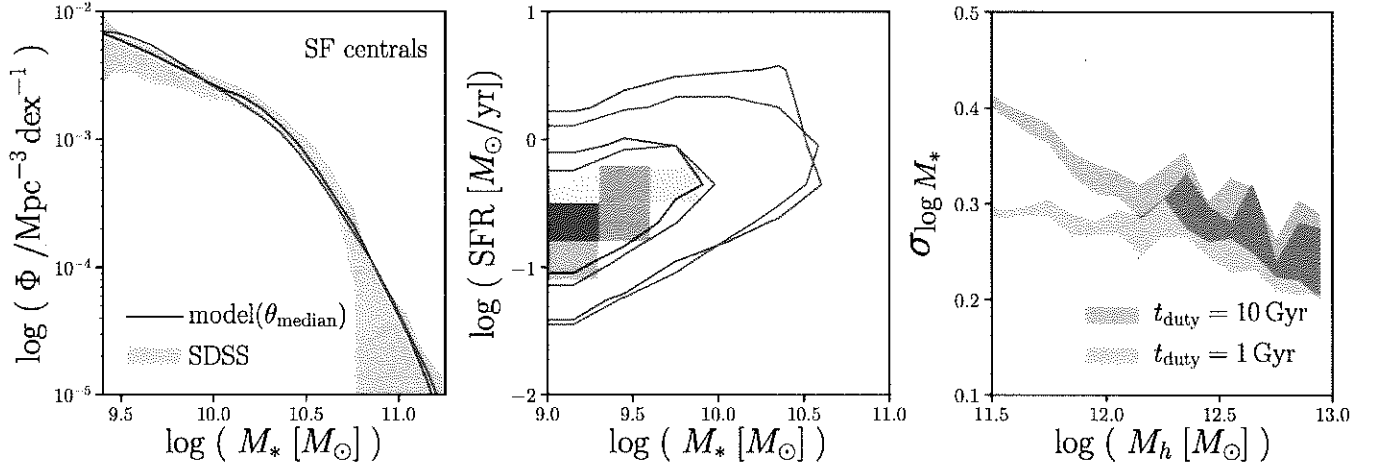


**Figure 5.** Our models with different star formation duty cycle timescales (blue:  $t_{\text{duty}}=1$  Gyr; red:  $t_{\text{duty}}=10$  Gyr) run with median values of their ABC posterior distribution produce SMFs and SFSs consistent with observations (left and middle). *They however predict significantly different scatter in  $\log M_*$  at fixed  $\log M_{\text{halo}}$  —  $\sigma_{\log M_*}$  (right).* By comparing the scatter in SHMR of our models to observational constraints on the SHMR, we can constrain the timescale of the star formation duty cycle and thereby the SFHs of star forming galaxies.

The SFHs in the middle and bottom panels illustrate this correlation and how  $\Delta \log \text{SFR}(t)$  correlates more strongly with  $\Delta M_h(t)$  for our model with higher  $r$ .

### 3.4. SHMR scatter at $z = 1$

So far in both our fiducial and galaxy assembly bias added models above, we assume that the log-normal scatter in  $M_*$  at fixed  $M_h$  at  $z \sim 1$ :  $\sigma_{\log M_*}^{\text{init}} = 0.2$  dex. This initial condition determines the initial SHAM  $M_*$  at  $z \sim 1$  that initializes our models and is motivated by constraints on the observed SHMR (*e.g.* Leauthaud et al. 2012; Tinker et al. 2013; Patel et al. 2015). However, these constraints are derived using halo models in which the scatter is a constant, independent of  $M_h$ . For these models, the constraining power mainly come from massive halos. Hence, the 0.2 dex constraint does not accurately reflect the SHMR scatter at  $z \sim 1$  for less massive halos ( $M_h \lesssim 10^{12} M_\odot$ ). Later in this paper, we focus on  $\sigma_{\log M_*}^{10^{12} M_\odot}$  at  $z = 0$ ) predicted by our models. We therefore examine the impact of varying  $\sigma_{\log M_*}^{\text{init}}$  on  $\sigma_{\log M_*}^{10^{12} M_\odot}$  using models with  $\sigma_{\log M_*}^{\text{init}} = 0.35$  and 0.45 dex. Our choice of  $\sigma_{\log M_*}^{\text{init}}$  is based on the  $z = 1$  SHMR in the Illustris TNG which has  $\sigma_{\log M_*}(z \sim 1)$  spanning 0.45 to 0.3 dex for  $M_h = 10^{11.5}$  to  $10^{12} M_\odot$ .

All of the models we present in this section track the SFRs and  $M_*$  of SF central galaxies. We can compare these properties of our model galaxies to observed galaxy population statistics (quiescent fraction and SMF) to constrain the free parameters. Our models, run with these inferred parameters, can then be compared to observations of the galaxy-halo connection such as the SHMR. In the following section, we present this comparison and the constraints we derive on the role and timescale of star formation variability in SF central galaxies.

## 4. RESULTS AND DISCUSSION

Our models take `TreePM` central subhalos and tracks their SFR and  $M_*$  evolution using flexible parameterizations of the SFS and SFHs that incorporate variability through a star formation duty cycle. At  $z = 0.05$ , the final timestep, our models predict SFR and  $M_*$  of SF centrals, along with their host halo properties. We now use these resulting properties to compare our model to observations and constrain its free parameters — the SFS parameters of Eq. 2. Since we focus on SF centrals, we use the SMF of SF centrals in SDSS, which we estimate as

$$\Phi_{\text{SF, cen}}^{\text{SDSS}} = f_{\text{SFS}}^{\text{cen}} \times f_{\text{cen}} \times \Phi^{\text{Li\&White(2009)}}. \quad (5)$$

$f_{\text{SFS}}^{\text{cen}}$  is the fraction of central galaxies on the SFS, which we fit in Eq. 1.  $f_{\text{cen}}$  is the central galaxy fraction from Wetzel et al. (2013) and  $\Phi^{\text{Li\&White(2009)}}$  is the SMF of the SDSS from Li & White (2009). If our models reproduce the observed  $\Phi_{\text{SF, cen}}^{\text{SDSS}}$ , by construction they reproduce the observed quiescent fraction.

For the comparison between our models and observation, we use the likelihood-free parameter inference framework of Approximate Bayesian Computation (ABC). ABC has the advantage over standard approaches to parameter inference in that it does not require evaluating the likelihood. For observables with likelihoods that are difficult or intractable, incorrect assumptions in the likelihood can significantly bias the posterior distributions (*e.g.* Hahn et al. 2018a). Instead, ABC relies only on a simulation of the observed data and a distance metric to quantify the “closeness” between the observed data and simulation. Many variations of ABC has been used in astronomy and cosmology (*e.g.* Cameron & Pettitt 2012; Weyant et al. 2013; Ishida et al. 2015; Alsing et al. 2018). We use ABC in conjunction with the efficient Population Monte Carlo (PMC) importance sampling as in Hahn et al. (2017a,b). For initial sampling of our ABC particles, *i.e.* the priors of our free parameters  $m_{M_*}^{\text{low}}$ ,  $m_{M_*}^{\text{high}}$ , and  $m_z$ , we use uniform distributions over the ranges  $[0.0, 0.8]$ ,  $[0.0, 0.8]$ , and  $[0.5, 2.]$ , respectively. The range of the prior were conservatively chosen to encompass the best-fit SFS from Speagle et al. (2014) as well as measurements from Moustakas et al. (2013) and Lee et al. (2015) at  $z \sim 1$ . Finally, for our distance metric we use the following distance between the SMF of the star-forming centrals in our model to the observed  $\Phi_{\text{SF, cen}}^{\text{SDSS}}$ :

$$\rho_{\Phi} = \sum_M \left( \frac{\Phi^{\text{sim}} - \Phi_{\text{SF, cen}}^{\text{SDSS}}}{\sigma'_{\Phi}} \right)^2. \quad (6)$$

$\Phi^{\text{sim}}(M)$  above is the SMF of the SF centrals in our model and  $\sigma'_{\Phi}(M)$  is the uncertainty of  $\Phi_{\text{SF, cen}}^{\text{SDSS}}$ , which we derive by scaling the Li & White (2009) uncertainty of  $\Phi^{\text{SDSS}}$  derived from mock catalogs. For the rest of our ABC-PMC implementation, we strictly follow the implementation of Hahn et al. (2017b) and Hahn et al. (2017a). We refer reader to those papers for further details.

### 4.1. The Fiducial Model

We present the SMFs (left), SFSs (center), and  $\sigma_{\log M_*}(M_h)$  (right) of our fiducial model run using SFHs with  $t_{\text{duty}} = 10$  (red) and 1 Gyr (blue) duty cycle timescales in Figure 5.  $\sigma_{\log M_*}(M_h)$  is the

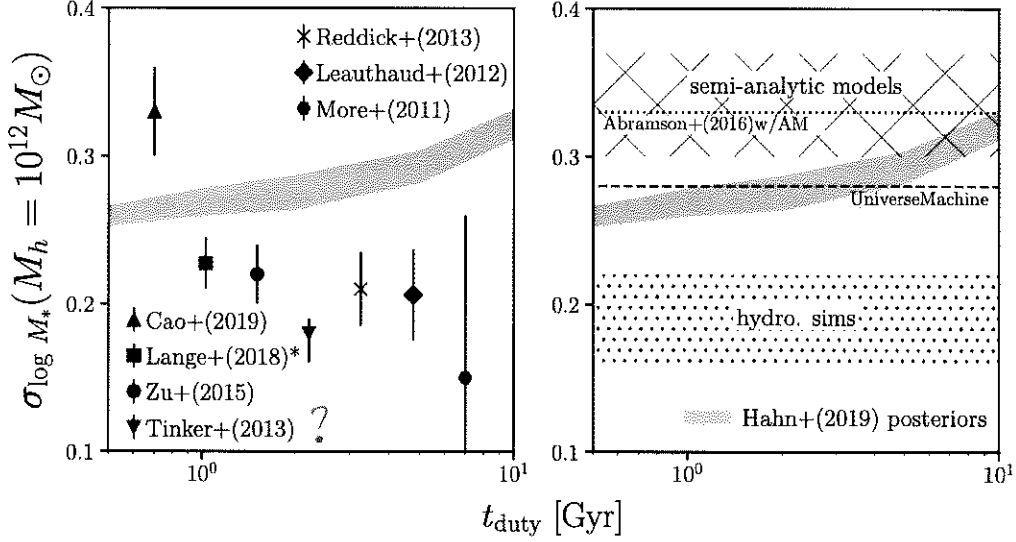


**Figure 6.** With shorter star formation duty cycle timescales,  $t_{\text{duty}}$ , our fiducial model predicts smaller scatter in  $\log M_*$  at  $M_h = 10^{12} M_\odot$  —  $\sigma_{\log M_*}^{10^{12} M_\odot}$  (blue). The dark and light blue shaded regions represent the 68% and 95% confidence intervals of the predicted scatter from the ABC posteriors of our model with  $t_{\text{duty}} = 0.5, 1, 2, 5$ , and 10 Gyr. For  $t_{\text{duty}} = 10$  to 0.5 Gyr,  $\sigma_{\log M_*}^{10^{12} M_\odot}$  ranges from  $0.32^{+0.02}_{-0.02}$  to  $0.26^{+0.01}_{-0.01}$ . In the left panel, we include for comparison observational  $\sigma_{\log M_*}$  constraints from Yang et al. (2009); More et al. (2011); Leauthaud et al. (2012); Zu & Mandelbaum (2015); Tinker et al. (2017b); Lange et al. (2018) and Cao et al. (in preparation), described in Section 4.1. In the right panel, we include compiled predictions from hydrodynamic simulations (dotted region), semi-analytic models (hatched), and the Behroozi et al. (2018) UM empirical model. We also include  $\sigma_{\log M_*}(M_h = 10^{12.4} M_\odot)$  from a simple empirical model with Abramson et al. (2016) SFHs assigned to halos via abundance matching (dotted). *A shorter  $t_{\text{duty}}$  produces significantly tighter scatter in the SHMR. Halo model observations constraints and predictions from hydrodynamic simulations favor a star formation variability on  $t_{\text{duty}} \lesssim 0.5$  Gyr for our fiducial model.*

scatter in  $\log M_*$  for halos of a given  $M_h$  — *i.e.* scatter in the SHMR. For each  $t_{\text{duty}}$ , we evaluate our fiducial model using the median values of the posterior parameter distributions derived from ABC. For both  $t_{\text{duty}}$ , our model successfully produces SMFs,  $\Phi_{\text{SF, cen}}^{\text{SDSS}}$ , and SFSs consistent with observations (left and center panels). Despite reproducing observations, however, with different  $t_{\text{duty}}$  the fiducial model predicts significantly different  $\sigma_{\log M_*}$ , particularly below  $M_h < 10^{12.5} M_\odot$ . We further illustrate the sensitivity of  $\sigma_{\log M_*}$  predicted by our model to  $t_{\text{duty}}$  in Figure 6, where we present  $\sigma_{\log M_*}$  at fixed halo mass  $M_h = 10^{12} M_\odot$  for our model with  $t_{\text{duty}} = 0.5, 1, 2, 5$ , and 10 Gyr.  $\sigma_{\log M_*}$  at each  $t_{\text{duty}}$  is the prediction from our model run using parameters from the corresponding ABC posterior distributions. The dark and light blue shaded regions represents the 68% and 95% confidence intervals. For  $t_{\text{duty}} = 10$  to 0.5 Gyr,  $\sigma_{\log M_*}^{10^{12} M_\odot}$  ranges from  $0.32^{+0.02}_{-0.02}$  to  $0.26^{+0.01}_{-0.01}$  — a shorter star formation duty cycle timescale produces significantly smaller scatter in the SHMR. Hence, *the SHMR, in particular  $\sigma_{\log M_*}^{10^{12} M_\odot}$ , can be used to probe the star formation variability timescale and SFH of SF central galaxies.*

On the left panel of Figure 6, we compare  $\sigma_{\log M_*}$  predictions from our fiducial model to observational constraints in the literature. These constraints are mainly derived from fitting halo-occupation

based models to observations of galaxy clustering, SMF, satellite kinematics, or galaxy-galaxy weak lensing. We include  $\sigma_{\log M_*}$  constraints from More et al. (2011); Leauthaud et al. (2012); Reddick et al. (2013); Tinker et al. (2013); Zu & Mandelbaum (2015) and Cao et al. (in preparation). More et al. (2011), Reddick et al. (2013), and Zu & Mandelbaum (2015) fit SDSS DR7 measurements of satellite kinematics, projected galaxy clustering and conditional SMF, and galaxy clustering and galaxy-galaxy lensing, respectively. Meanwhile, Leauthaud et al. (2012); Tinker et al. (2013) use COSMOS to fit the SMF, galaxy clustering, and galaxy-galaxy lensing. Finally, Cao et al. (in preparation) fit the kurtosis of the line-of-sight pairwise velocity dispersion between central galaxies and all neighboring galaxies to constrain the scatter in SHMR at low halo masses. We note that Leauthaud et al. (2012); Reddick et al. (2013); Zu & Mandelbaum (2015) measure  $\sigma_{\log M_*}$  for all central galaxies, not only SF. Both More et al. (2011); Tinker et al. (2013), however, find a  $< 1\sigma$  difference in  $\sigma_{\log M_*}$  between SF and quiescent centrals, so we include these constraints in our comparison. We also include the Lange et al. (2018) constraint from fitting color-dependent conditional luminosity function and radial profile of satellite galaxies of SDSS DR7. This constraint, however, is on the scatter in luminosity,  $\log L$ , not  $\log M_*$  at a given  $M_h$ .

Overall, observational constraints are more consistent with  $\sigma_{\log M_*}$  predictions of our fiducial model with a short,  $< 1$  Gyr, duty cycle timescale. However, there is no clear consensus among the observed  $\sigma_{\log M_*}$  constraints. Besides Cao et al. (in preparation), the  $\sigma_{\log M_*}$  constraints in the literature are loosely consistent with  $\sim 0.2$  dex. These constraints, however, are mostly derived using halo models that assume  $\sigma_{\log M_*}$  is a constant, independent of  $M_h$ . The constraining power for these constraints mainly come from high mass halos and, thus, do not reflect  $\sigma_{\log M_*}$  at  $M_h = 10^{12} M_\odot$ . While Reddick et al. (2013) constrain  $\sigma_{\log M_*}$  for different bins of  $M_h$  over the range  $10^{12} - 10^{14} M_\odot$ , their constraints mainly come from the conditional SMF and therefore relies on the accuracy of the Tinker et al. (2011) group finder in identifying halo masses. CH: JLT: Why does Reddick come from  $10^{13} M_\odot$ ? The constraint from Lange et al. (2018) is also derived from a halo model with  $M_h$  dependence. However, as mentioned above, they constrain  $\sigma_{\log L}$ . In More et al. (2011), where they constrain both  $\sigma_{\log L}$  and  $\sigma_{\log M_*}$  from the same sample, they find  $\sigma_{\log M_*} = 0.15^{+0.08}_{-0.11} < \sigma_{\log L} = 0.21^{+0.06}_{-0.04}$  for blue centrals. Translating  $\sigma_{\log L}$  to  $\sigma_{\log M_*}$ , however, is tenuous for different data sets and models. We also note observational constraints include significant measurement uncertainties in  $M_*$ . The intrinsic  $\sigma_{\log M_*}$  of these constraints, *i.e.* the scatter predicted by our model, will be lower. If we consider  $0.1 - 0.2$  dex uncertainties in  $M_*$  (Roediger & Courteau 2015), the Cao et al. (in preparation) constraint, for instance, will be reduced from  $\sigma_{\log M_*} = 0.33$  dex to  $0.31 - 0.26$  dex.

In addition to the observational constraints, we also compare the  $\sigma_{\log M_*}^{10^{12} M_\odot}$  predicted by our model to predictions from modern galaxy formation models on the right panel: hydrodynamic simulations (dot filled), semi-analytic models (SAM; hatched), and an empirical model (dashed line). For the hydrodynamic simulations, the dotted region,  $\sigma_{\log M_*}^{M_h=10^{12} M_\odot} = 0.16 - 0.22$  dex, encompasses predictions from EAGLE (Matthee et al. 2017), Massive Black II (Khandai et al. 2015), and Illustris TNG, as compiled in Figure 8 of Wechsler & Tinker (2018). For the SAMs, the hatched region,  $\sigma_{\log M_*}^{M_h=10^{12} M_\odot} =$

0.3 – 0.37 dex, includes predictions from Lu et al. (2014); Somerville et al. (2012) and the SAGE<sup>2</sup> model (Croton et al. 2016). We also include the prediction from the Behroozi et al. (2018) UM empirical model. Similar to observations, there is little consensus among the  $\sigma_{\log M_*}$  predictions of the galaxy formation models.  $\sigma_{\log M_*}$  from SAMs are consistent with our model with  $t_{\text{duty}} \gtrsim 5$  Gyr. UM, which predicts a lower  $\sigma_{\log M_*}$ , is consistent with  $t_{\text{duty}} = 1 - 5$  Gyr. Lastly, hydrodynamic simulations predict the lowest  $\sigma_{\log M_*}$  among the models with  $\sim 0.2$  dex, which our fiducial model struggles to reproduce even with  $t_{\text{duty}} = 0.5$  Gyr. We note that while there is yet no consensus among the observational  $\sigma_{\log M_*}$  constraints at  $M_h = 10^{12} M_\odot$ , at higher  $M_h$  observations are in better agreement and *only* hydrodynamic simulations predict  $\sigma_{\log M_*}$  consistent with these observations (Wechsler & Tinker 2018). Right below  $M_h = 10^{12} M_\odot$ , however, hydrodynamic simulations predict significantly higher scatter —  $\sigma_{\log M_*}(M_h \sim 10^{11.5}) = 0.22 - 0.32$  dex (Wechsler & Tinker 2018).

Given the little consensus among the actual  $\sigma_{\log M_*}$  constraints at  $z = 0$  from both observations and simulations, we examine the more quantitative redshift evolution trend of  $\sigma_{\log M_*}$  from  $z = 1$  to 0. For our model  $\sigma_{\log M_*}$  at  $z = 1$  is an input initial condition we use to determine the initial SHAM  $M_*$  of our model that we set to 0.2 dex, based on halo model observations (*e.g.* Leauthaud et al. 2012; Tinker et al. 2013; Patel et al. 2015). According to our  $\sigma_{\log M_*}(z = 0)$  predictions,  $\sigma_{\log M_*}^{10^{12} M_\odot}$  increases by 0.06 – 0.12 dex for  $t_{\text{duty}} = 1 - 10$  Gyr. In comparison, halo model observational constraints find constant  $\sigma_{\log M_*} = 0.2$  dex evolution. Meanwhile in Illustris TNG, (Cao et al. (in preparation)) find that  $\sigma_{\log M_*}^{10^{12} M_\odot}$  actually decreases over the redshift range from  $\sim 0.3$  dex at  $z = 1$  to  $\sim 0.2$  dex at  $z = 0$ . Both of these  $\sigma_{\log M_*}$  evolution trends, despite their difference, favor a short duty cycle. However, even with the shortest duty cycle, we find an increasing  $\sigma_{\log M_*}^{10^{12} M_\odot}$  from  $z = 1$ . *Q not here at end.*

A key element of our models is the SFH prescription for SF central galaxies where the SFH evolves about the SFS. Contrary to our SFH prescription, Kelson (2014), for example, argue that the SFS is a consequence of central limit theorem and can be reproduced even if *in situ* stellar mass growth is modeled as a stochastic process like a random walk. Gladders et al. (2013); Abramson et al. (2015, 2016), similarly argue that  $\sim 2000$  loosely constrained log-normal SFHs can reproduce observations such as the SMF at  $z \leq 8$  and the SFS at  $z \leq 6$ . These works, however, focus on reproducing observations of galaxy properties and do not examine the galaxy-halo connection such as the SHMR. In order to test whether log-normal SFHs can also produce realistic SHMRs, we construct a simple empirical model using the SFHs, SFR( $t$ ) and  $M_*(t)$ , from Abramson et al. (2016) and assign them to halos by abundance matching their  $M_*$  to  $M_h$  at  $z \sim 1$ . We then restrict the SFHs to those that would be classified as star-forming based on a  $\log \text{SSFR} > -11$  cut. Afterwards we measure  $\sigma_{\log M_*}$  at the lowest  $M_h$  where it can be reliably measured given the Abramson et al. (2016) sample's  $M_* > 10^{10} M_\odot$  limit. We find that the Abramson et al. (2016) based empirical model predicts a scatter of  $\sigma_{\log M_*}(M_h = 10^{12.4} M_\odot) = 0.33 \pm 0.04$  (dotted; right panel of Figure 6). Although the Abramson et al. (2016) SFHs can reproduce various galaxy properties, the empirical model we construct with them struggles to produce  $\sigma_{\log M_*}$  comparable to observational constraints and predictions from UM and hydrodynamic simulations. It also struggles to keep  $\sigma_{\log M_*}$  evolution constant or decreasing

<sup>2</sup> <https://tao.asvo.org.au/tao/>

*make  
log-normal  
a distinct  
subsection.  
or cut.*



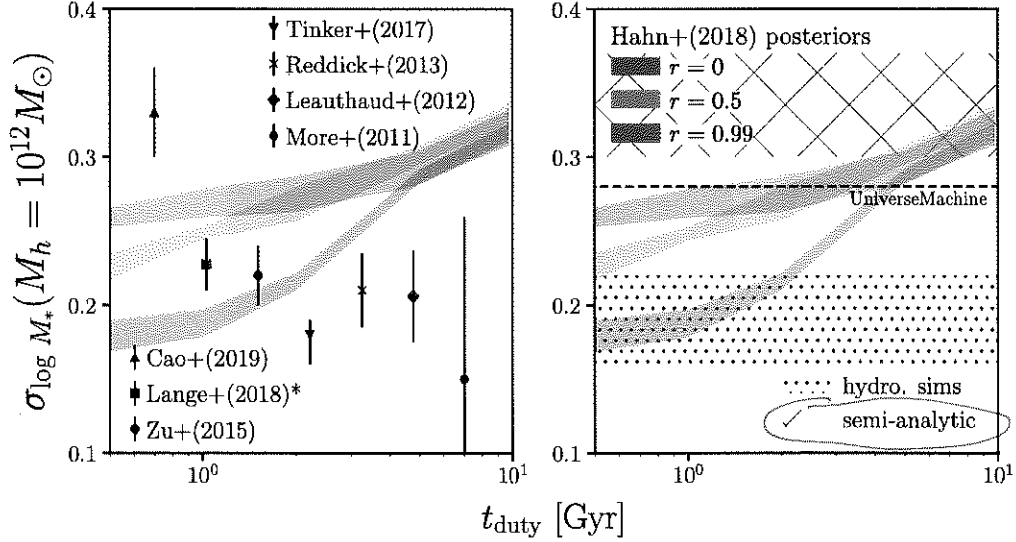


**Figure 7.** Using models that correlate SFH with halo assembly history, we find that higher  $r$ , *i.e.* stronger galaxy assembly bias, significantly reduces the scatter in SHMR for  $t_{\text{duty}} < 5$  Gyr. We plot  $\sigma_{\log M_*}(M_h = 10^{12} M_\odot)$  as a function of the star formation duty cycle timescale,  $t_{\text{duty}}$ , for our models with  $r = 0$  (no assembly bias; blue), 0.5 (orange), and 0.99 (green). We include observational constraints and predictions from galaxy formation models in the left and right panels, respectively. With  $r > 0.5$ , our models can predict  $\sigma_{\log M_*}(M_h = 10^{12} M_\odot)$  more consistent with the tight  $\sim 0.2$  dex constraint from halo model observations and hydrodynamic simulations.  $r > 0$  also reduces the growth in  $\sigma_{\log M_*}(M_h = 10^{12} M_\odot)$  evolution from  $z = 1$  to 0.

with redshift. The Abramson et al. (2016) based empirical model that we explore utilizes a simple abundance matching scheme. Diemer et al. (2017) find that their log-normal fits to the SFHs of Illustris galaxies correlate with halo formation histories. Incorporating such correlations into the abundance matching may reduce  $\sigma_{\log M_*}$ .

In this section we demonstrate that star formation variability in the SFH impacts  $\sigma_{\log M_*}(M_h = 10^{12} M_\odot)$ : star formation variability on shorter timescales significantly reduces  $\sigma_{\log M_*}(M_h = 10^{12} M_\odot)$ . Given this dependence,  $\sigma_{\log M_*}$  can conversely be used to constrain the timescale of star formation variability. Although there is no clear consensus in the  $\sigma_{\log M_*}(M_h = 10^{12} M_\odot)$  of observations or simulations, overall they favor our model with short variability timescales  $\sim 0.5$  Gyr. However, we find that star formation variability alone is insufficient in producing the tight SHMR scatter and  $\sigma_{\log M_*}$  redshift evolution trend found in halo model observations and hydrodynamic simulations. In the next section, we explore how correlation between SFH and halo formation histories impacts  $\sigma_{\log M_*}(M_h = 10^{12} M_\odot)$  using our models with galaxy assembly bias.

#### 4.2. Models with Assembly Bias: $r > 0$

A shorter star formation duty cycle timescale produces tighter scatter in the SHMR of our fiducial model. This dependence on the duty cycle timescale, allows us to compare the model with measurements of  $\sigma_{\log M_*}(M_h = 10^{12} M_\odot)$  and predictions from galaxy formation models to constrain  $t_{\text{duty}}$ , which reflect the star formation variability timescale. Such comparisons in the previous section, demonstrate

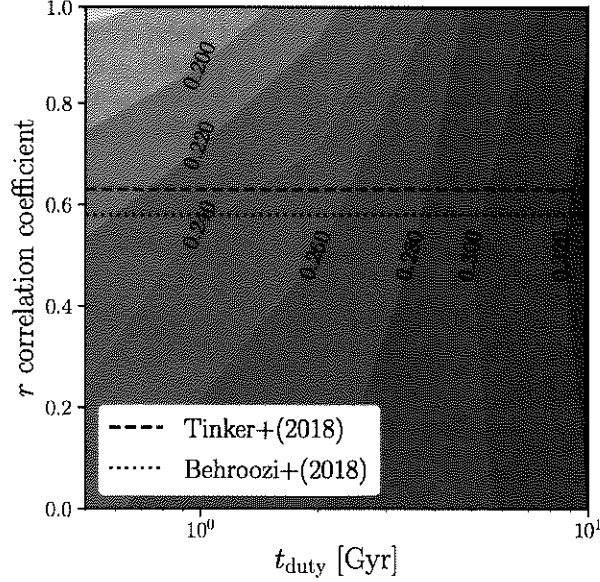


**Figure 8.** Predicted  $\sigma_{\log M_*}$  as a function of  $t_{\text{duty}}$  and  $r$  for our models illustrate the degeneracy between the timescale of SF variability and the correlation between SFH and halo assembly history. Based on  $r$  constraints from Tinker et al. (2018a) (dashed) and Behroozi et al. (2018) (dotted),  $t_{\text{duty}} < 0.5$  Gyr is necessary to produce  $\sigma_{\log M_*} \sim 0.2$  dex from observations and hydrodynamic simulations. Meanwhile,  $t_{\text{duty}} < 5$  Gyr is necessary to produce  $\sigma_{\log M_*}$  from Cao et al. (in preparation), SAMs, and UM.

that  $t_{\text{duty}} \lesssim 0.5$  Gyr is favored by observational constraints. However, a short duty cycle timescale alone is not enough to reproduce  $\sigma_{\log M_*}$  constraints and its evolutionary trend from halo model observations and hydrodynamic simulations. In this section, we examine how assembly bias impacts  $\sigma_{\log M_*}$  using our models that correlate SFH with host halo accretion history ( $r > 0$ ).

We repeat our analysis of inferring model parameters by comparing to observations using ABC-PMC — this time for our model with galaxy assembly bias over a grid of  $t_{\text{duty}}$  and  $r$  values. Using the resulting posterior distributions, we examine  $\sigma_{\log M_*}^{10^{12} M_\odot}$  predicted by our model as a function of  $t_{\text{duty}}$  with  $r = 0$  (no assembly bias; blue), 0.5 (orange), and 0.99 (green) in Figure 7. The shaded regions represent the 68% confidence interval of the predicted  $\sigma_{\log M_*}^{10^{12} M_\odot}$ . We again emphasize that for all sets of  $(t_{\text{duty}}, r)$  our models reproduce the observed SMF of SF centrals and SFS. At  $t_{\text{duty}} \geq 5$  Gyr we find no significant difference in the scatter, regardless of  $r$ . Below  $t_{\text{duty}} < 5$  Gyr, however,  $\sigma_{\log M_*}^{10^{12} M_\odot}$  of our model decreases significantly as the SFH of SF galaxies are more correlated with halo accretion history. For  $t_{\text{duty}} = 0.5$  Gyr, we find  $\sigma_{\log M_*}^{10^{12} M_\odot} = 0.26^{+0.01}_{-0.01}$ ,  $0.22^{+0.01}_{-0.01}$ , and  $0.17^{+0.01}_{-0.02}$  for  $r = 0.0, 0.5$ , and 0.99, respectively.

Comparing our  $r > 0$  models to the observational constraints, we find that galaxy assembly bias significantly reduces the tensions with halo model observations (left panel of Figure 7). With a short star formation duty cycle ( $t_{\text{duty}} \leq 1$  Gyr) and galaxy assembly bias with  $r \geq 0.5$ , our model is in agreement with these  $\sigma_{\log M_*} \sim 0.2$  dex constraints. On the other hand, assembly bias increases the tension with Cao et al. (in preparation), which more specifically constrains  $\sigma_{\log M_*}$  at  $M_h \sim 10^{12} M_\odot$ . We also compare our  $r > 0$  models to predictions from galaxy formation models on the right panel.

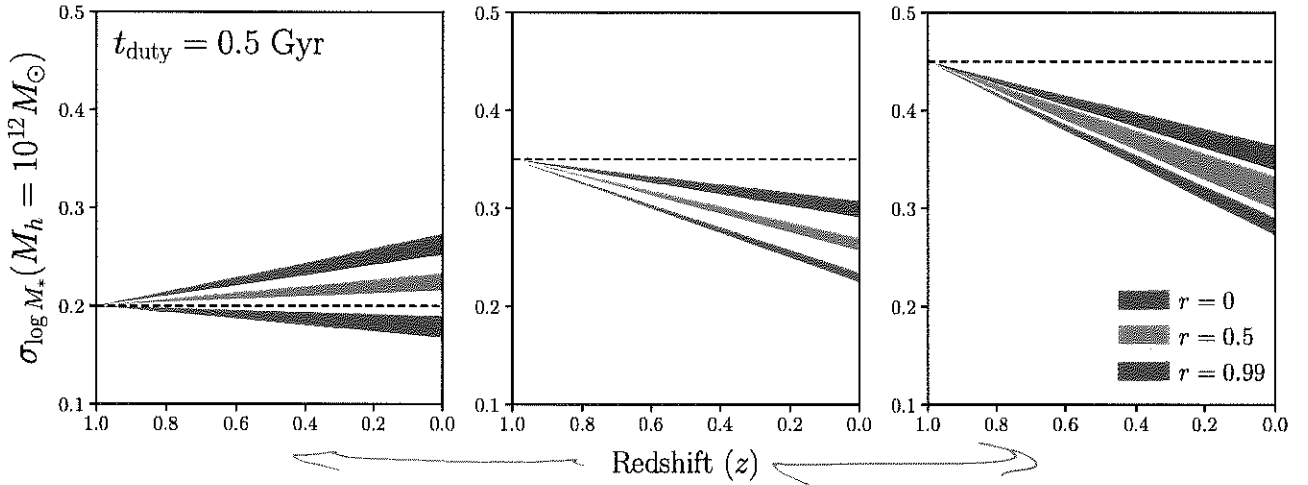


**Figure 9.** The evolution of  $\sigma_{\log M_*}^{10^{12} M_\odot}$  from  $z = 1$  to 0 for our models with  $t_{\text{duty}} = 0.5$  Gyr and  $r = 0$  (blue), 0.5 (orange), and 0.99 (green). In each panel we vary the initial  $\sigma_{\log M_*}^{10^{12} M_\odot}$  at  $z = 1$ ,  $\sigma_{\log M_*}^{\text{init}} = 0.2, 0.35$ , and 0.45 dex (left, center, and right panels, respectively).  $\sigma_{\log M_*}^{\text{init}} = 0.35$  and 0.45 dex are motivated by  $\sigma_{\log M_*}$  at  $M_h = 10^{12}$  and  $10^{11.5} M_\odot$ , respectively, in the Illustris TNG (Cao et al. (in preparation)). The width of the shaded region represent the 68% confidence interval. We mark  $\sigma_{\log M_*}^{\text{init}}$  in black dashed. Increasing  $\sigma_{\log M_*}^{\text{init}}$ , increases  $\sigma_{\log M_*}^{10^{12} M_\odot}$  overall. However, for all  $\sigma_{\log M_*}^{\text{init}}$ ,  $r > 0$  reduces the  $\sigma_{\log M_*}^{10^{12} M_\odot}$  evolution. For the  $\sigma_{\log M_*}^{\text{init}} > 0.2$  dex models, even without galaxy assembly bias ( $r = 0$ ),  $t_{\text{duty}} = 0.5$  Gyr alone significantly tightens  $\sigma_{\log M_*}^{10^{12} M_\odot}$  from  $z = 1$  to 0 (blue). This is enhanced with  $r > 0$ . With  $r \geq 0.5$ , the  $\sigma_{\log M_*}^{\text{init}} > 0.2$  dex models can produce  $\sigma_{\log M_*}^{10^{12} M_\odot}$  evolutions consistent with the  $\sim 0.15$  dex decline in  $\sigma_{\log M_*}^{10^{12} M_\odot}$  Cao et al. (in preparation) find in Illustris TNG.

By varying  $r$  and  $t_{\text{duty}}$ , our model can reproduce the widely varying galaxy formation model  $\sigma_{\log M_*}^{10^{12} M_\odot}$  predictions. Focusing on hydrodynamic simulations, which best reproduce  $\sigma_{\log M_*}$  observations at high  $M_h$ , we find that with a short duty cycle timescale,  $t_{\text{duty}} < 1$  Gyr, and  $r > 0.5$  our models produces the predicted  $\sim 0.2$  dex scatter in SHMR.

A shorter  $t_{\text{duty}}$  or higher  $r$  both produce smaller  $\sigma_{\log M_*}^{10^{12} M_\odot}$ . We highlight this degeneracy in Figure 8, where we plot  $\sigma_{\log M_*}$  at  $M_h = 10^{12} M_\odot$  (contour and color map) as a function of  $t_{\text{duty}}$  and  $r$ . Figure 8 more precisely reveals that to produce  $\sigma_{\log M_*} \sim 0.2$  dex  $t_{\text{duty}} \leq 1.5$  Gyr and  $r > 0.7$  (top left corner of Figure 8). In the literature, Tinker et al. (2018a) find correlation between  $\dot{M}_h$  and log SSFR with  $r = 0.63$  (dashed) and Behroozi et al. (2018) similarly find a correlation between SFH and halo assembly history with  $r_c \sim 0.6$  for halos with  $M_h \sim 10^{12} M_\odot$  (dotted). For galaxy assembly bias with  $r = 0.6$ , even with the shortest timescale we probe ( $t_{\text{duty}} = 0.5$  Gyr) our model struggles to produce  $\sigma_{\log M_*}^{10^{12} M_\odot} \sim 0.2$  dex as found in halo model observations and hydrodynamic simulations, which suggests that SF variability on timescales  $< 0.5$  Gyr is necessary. This timescale is shorter than the  $\sim 0.5$  Gyr timescale that Sparre et al. (2015) find in Illustris galaxies using a Principal Component Analysis of the SFHs. However, it is consistent with the shorter  $\sim 0.1$  Gyr timescales found in the FIRE simulations (Hopkins et al. 2014; Sparre et al. 2017).

We examine the evolutionary trend of  $\sigma_{\log M_*}^{10^{12}M_\odot}$  in Figure 9, where we plot  $\sigma_{\log M_*}^{10^{12}M_\odot}$  from  $z = 1$  to 0 for our model with  $t_{\text{duty}} = 0.5$  Gyr and  $r = 0$  (blue), 0.5 (orange), and 0.99 (green). The width of the shaded region represent the 68% confidence interval. We mark the initial  $\sigma_{\log M_*}^{10^{12}M_\odot}$ ,  $\sigma_{\log M_*}^{\text{init}}$ , in black dashed;  $\sigma_{\log M_*}^{\text{init}} = 0.2, 0.35$ , and  $0.45$  dex in the left, center, and right panels, respectively. Focusing on the  $\sigma_{\log M_*}^{\text{init}} = 0.2$  panel (left), we find that for  $r > 0$  reduces the growth in  $\sigma_{\log M_*}^{10^{12}M_\odot}$  from  $\sigma_{\log M_*}^{\text{init}}$ . For  $r = 0.99$ , we see that our model (green) predicts  $\sigma_{\log M_*}^{10^{12}M_\odot}$  that decreases from  $\sigma_{\log M_*}^{\text{init}} = 0.2$  dex.  $r = 0.99$ , however, is inconsistent with constraints from the literature. For  $r \sim 0.6$  (Behroozi et al. 2018; Tinker et al. 2018a), we find a slight growth in  $\sigma_{\log M_*}^{10^{12}M_\odot}$  from  $z = 1$ :  $\sim 0.02$  dex (Figures 8 and 9). This is loosely consistent with halo model observational constraints that find constant  $\sigma_{\log M_*} = 0.2$  dex evolution. However, as we discuss in Section 3.4, the constant  $\sigma_{\log M_*} = 0.2$  dex evolution from halo model observations is based on  $\sigma_{\log M_*}^{\text{init}} = 0.2$  dex constraints in the literature, which do not accurately reflect the SHMR scatter at  $z \sim 1$  at  $M_h = 10^{12}M_\odot$ .

Relaxing the  $\sigma_{\log M_*}^{\text{init}} = 0.2$  dex assumption, we present the  $\sigma_{\log M_*}^{10^{12}M_\odot}$  evolution for our models with  $\sigma_{\log M_*}^{\text{init}} = 0.35$  and  $0.45$  dex (center and right panels of Figure 9).  $\sigma_{\log M_*}^{\text{init}} = 0.35$  and  $0.45$  dex is motivated by  $\sigma_{\log M_*}$  at  $M_h = 10^{12}$  and  $10^{11.5}M_\odot$ , respectively, in Illustris TNG (Cao et al. (in preparation)). Increasing  $\sigma_{\log M_*}^{\text{init}}$ , increases  $\sigma_{\log M_*}^{10^{12}M_\odot}$  overall for all  $r$ . However, both a shorter  $t_{\text{duty}}$  and higher  $r$  produce tighter  $\sigma_{\log M_*}^{10^{12}M_\odot}$  in our  $\sigma_{\log M_*}^{\text{init}} > 0.2$  dex models. Hence,  $\sigma_{\log M_*}^{10^{12}M_\odot}$  remains sensitive to  $t_{\text{duty}}$  and  $r$ , regardless of  $\sigma_{\log M_*}^{\text{init}}$ . Figure 9 illustrates that for the  $\sigma_{\log M_*}^{\text{init}} > 0.2$  dex models, even without galaxy assembly bias ( $r = 0$ ),  $t_{\text{duty}} = 0.5$  Gyr alone significantly tightens  $\sigma_{\log M_*}^{10^{12}M_\odot}$  from  $z = 1$  to 0 (blue):  $\sim 0.05$  and  $0.1$  dex for  $\sigma_{\log M_*}^{\text{init}} = 0.35$  and  $0.45$  dex, respectively. With  $r > 0$ , the decline in  $\sigma_{\log M_*}^{10^{12}M_\odot}$  from  $z = 1$  to 0 is further enhanced. With  $r \geq 0.5$ , the  $\sigma_{\log M_*}^{\text{init}} > 0.2$  dex models can produce  $\sigma_{\log M_*}^{10^{12}M_\odot}$  evolutions consistent with the  $\sigma_{\log M_*}^{10^{12}M_\odot}$  decline Cao et al. (in preparation) find in the Illustris TNG.

In this section, we use our models with different  $t_{\text{duty}}$ ,  $r$ , and  $\sigma_{\log M_*}^{\text{init}}$  to investigate how these parameters impact predictions of  $\sigma_{\log M_*}^{10^{12}M_\odot}$  at  $z = 0$ . A shorter timescale of star formation variability,  $t_{\text{duty}}$ , produces a tighter SHMR scatter. Similarly, higher correlation between SFH and halo assembly history, higher  $r$ , also produces a tighter SHMR scatter. Furthermore,  $\sigma_{\log M_*}^{10^{12}M_\odot}$  remains sensitive to  $t_{\text{duty}}$  and  $r$ , regardless of  $\sigma_{\log M_*}^{\text{init}}$ . Comparing our model predictions to  $\sigma_{\log M_*}^{10^{12}M_\odot}$  constraints in the literature, we find that by varying  $t_{\text{duty}}$  and  $r$  our model can produce  $\sigma_{\log M_*}^{10^{12}M_\odot}$  loosely consistent with constraints from observations and modern galaxy formation models, which span  $0.2 - 0.35$  dex. To reproduce the constant  $\sigma_{\log M_*} \sim 0.2$  dex evolution from  $z = 1$  to 0 found in halo model based observational constraints, our models require  $t_{\text{duty}} \leq 1.5$  Gyr for  $r = 0.99$  and  $r > 0.7$  for  $t_{\text{duty}} = 0.5$  Gyr. If we fix  $r = 0.6$ , the constraint on galaxy assembly bias from the literature,  $t_{\text{duty}} < 0.5$  Gyr is necessary. Meanwhile, to reproduce the  $\sigma_{\log M_*}^{10^{12}M_\odot} \sim 0.35$  to  $0.2$  dex decline from  $z = 1$  to 0 found in Illustris TNG, our models with  $\sigma_{\log M_*}^{\text{init}} > 0.2$  dex require  $r > 5$  for  $t_{\text{duty}} = 0.5$  Gyr. The lack of consensus among observations and galaxy formation models prevents us from precisely constraining  $t_{\text{duty}}$  or  $r$ . However, we illustrate that  $\sigma_{\log M_*}^{10^{12}M_\odot}$ , the scatter of the SHMR, is sensitive to  $t_{\text{duty}}$  and  $r$  and, thus, demonstrate that measurements of the SHMR relation can be used to constrain the detailed star formation histories of SF central galaxies and their connection to host halo assembly histories.

## 5. SUMMARY AND CONCLUSION

Despite our progress in understanding how galaxies form and evolve in the  $\Lambda$ CDM hierarchical universe, our understanding of the detailed star formation histories of galaxies and their connection to host halo assembly histories have been limited. This is in part due to the challenges in directly measuring SFHs in both observations and galaxy formation models. Empirical models, with their flexible prescriptions have made significant progress in better quantifying the SFHs of galaxies. These models, however, have yet to examine and constrain the timescale of star formation variability, which has the potential to constrain physical processes involved in star formation and galaxy feedback models. In this paper, we therefore focus on measuring the timescale of star formation variability and the connection between star formation and host halo accretion histories of star-forming central galaxies.

We combine the high-resolution cosmological  $N$ -body TreePM simulation with SFHs that evolve the SF central galaxies along the SFS and present models that tracks the SFR,  $M_*$ , and host halo accretion histories of SF centrals from  $z \sim 1$  to  $z = 0.05$ . More specifically, we characterize the SFHs to evolve with respect to the mean  $\log$  SFR of the SFS with a “star formation duty cycle” that introduces star formation variability on a specific timescale,  $t_{\text{duty}}$ . We parameterize the SFS using parameters that dictate the low  $M_*$  and high  $M_*$  slopes and redshift evolution. We then compare this model to the observed SMF of the SF centrals in the SDSS DR7 group catalog using ABC-PMC likelihood-free parameter inference framework. When we examine the SHMR predicted by the model and inferred parameters we find:

- A shorter star formation duty cycle in our model produces significantly tighter scatter in the SHMR at  $M_h = 10^{12} M_\odot$ ,  $\sigma_{\log M_*}^{10^{12} M_\odot}$ . For  $t_{\text{duty}}$  from 10 to 0.5 Gyr, our model predicts  $\sigma_{\log M_*}^{10^{12} M_\odot} = 0.32^{+0.019}_{-0.021}$  to  $0.26^{+0.010}_{-0.012}$ . The dependence of  $\sigma_{\log M_*}$  on  $t_{\text{duty}}$  demonstrates that the scatter in SHMR can be used to constrain  $t_{\text{duty}}$ , and thus the timescale of star formation variability.
- We compare the  $\sigma_{\log M_*}^{10^{12} M_\odot}$  predicted by our model to observed constraints from halo occupation modeling of galaxy clustering, SMF, satellite kinematics, and galaxy-galaxy weak lensing. There is significant tension among the observational constraints and also among predictions from galaxy formation models with  $\sigma_{\log M_*}^{10^{12} M_\odot}$  spanning 0.2 to 0.35 dex. Among the literature, constraints from halo model based observations and hydrodynamic simulations find  $\sigma_{\log M_*}^{10^{12} M_\odot} \sim 0.2$  dex, which our model struggles to produce even with the shortest timescale we probe,  $t_{\text{duty}} = 0.5$  Gyr.
- We next examine models with assembly bias that correlate SFHs to host halo accretion histories with correlation coefficient,  $r$ . With stronger correlation, higher  $r$ , our models predict tighter scatter in the SHMR down to  $\sigma_{\log M_*}^{10^{12} M_\odot} = 0.17$  for  $r = 0.99$ . To produce  $\sigma_{\log M_*}^{10^{12} M_\odot} \sim 0.2$  dex, our models require  $r > 0.7$  for  $t_{\text{duty}} = 0.5$  Gyr or  $t_{\text{duty}} < 2$  Gyr for  $r = 0.99$ . For  $r \sim 0.6$ , as found in the literature,  $t_{\text{duty}} \lesssim 0.5$  Gyr is necessary. If we allow  $\sigma_{\log M_*}^{\text{init}}$  at  $z = 1$  to vary  $> 0.2$  dex, we

find that our model requires  $t_{\text{duty}} = 0.5$  Gyr for  $r > 0.5$  to reproduce the  $\sigma_{\log M_*}^{10^{12} M_\odot} = 0.35$  to 0.2 dex evolution from  $z = 1$  to 0 in Illustris TNG.

Our work demonstrates that constraints on the scatter in the SHMR can be used to constrain both the timescale of star formation variability and the correlation between SFH and halo accretion history. The main bottleneck in deriving precise constraints on the timescale of star formation variability remains the lack of consensus among  $\sigma_{\log M_*}^{10^{12} M_\odot}$  observations both at  $z = 0$  and 1. Upcoming surveys, however, will make significant progress on this front.

The Bright Galaxy Survey of the Dark Energy Spectroscopic Instrument (DESI; Collaboration et al. 2016), for instance, will observe  $\sim 10$  million galaxies down to the magnitude limit  $r \sim 20$  out to  $z \sim 0.5$ . This will enable BGS to more precisely constrain  $\sigma_{\log M_*}$  and resolve current tensions in observations at  $z = 0$ . Meanwhile, the Galaxy Evolution Survey of the Prime Focus Spectrograph (Tamura et al. 2016), which will observe  $\sim 500,000$  galaxies between  $0.5 < z < 2$ , and the Wide-Area VISTA Extragalactic Survey (WAVES; ??), which will observe  $\sim 2$  million galaxies down to  $r_{\text{AB}} < 22$  mag out to  $z \sim 1$ , will enable precise constraints of  $\sigma_{\log M_*}$  at  $z \sim 1$ . Using measurements from these surveys, our model will be able to constrain the physical processes that govern star formation in galaxies and the detailed connection between star formation and host halo accretion.

## ACKNOWLEDGEMENTS

It's a pleasure to thank J.D. Cohn, Shirley Ho, and Tjitske Starkenburg for valuable discussions and feedback. We also thank Louis E. Abramson, Junzhi Cao, Shy Genel, and Cheng Li for providing us with data used in the analysis. This material is based upon work supported by the U.S. Department of Energy, Office of Science, Office of High Energy Physics, under contract No. DE-AC02-05CH11231.

## REFERENCES

- Abazajian, K. N., Adelman-McCarthy, J. K., Agüeros, M. A., et al. 2009, *The Astrophysical Journal Supplement Series*, 182, 543, doi: 10.1088/0067-0049/182/2/543
- Abramson, L. E., Gladders, M. D., Dressler, A., et al. 2016, *The Astrophysical Journal*, 832, 7, doi: 10.3847/0004-637X/832/1/7
- . 2015, *The Astrophysical Journal Letters*, 801, L12, doi: 10.1088/2041-8205/801/1/L12
- Alsing, J., Wandelt, B., & Feeney, S. 2018, arXiv:1801.01497 [astro-ph].  
<https://arxiv.org/abs/1801.01497>
- Artale, M. C., Zehavi, I., Contreras, S., & Norberg, P. 2018, *Monthly Notices of the Royal Astronomical Society*, 480, 3978, doi: 10.1093/mnras/sty2110
- Baldry, I. K., Balogh, M. L., Bower, R. G., et al. 2006, *Monthly Notices of the Royal Astronomical Society*, 373, 469, doi: 10.1111/j.1365-2966.2006.11081.x
- Becker, M. R. 2015, arXiv e-prints, 1507, arXiv:1507.03605
- Behroozi, P., Wechsler, R., Hearin, A., & Conroy, C. 2018, ArXiv e-prints, 1806, arXiv:1806.07893
- Behroozi, P. S., Wechsler, R. H., & Conroy, C. 2013, *The Astrophysical Journal*, 770, 57, doi: 10.1088/0004-637X/770/1/57
- Bekki, K. 2009, *Monthly Notices of the Royal Astronomical Society*, 399, 2221, doi: 10.1111/j.1365-2966.2009.15431.x
- Blanton, M. R. 2006, *The Astrophysical Journal*, 648, 268, doi: 10.1086/505628

- Blanton, M. R., & Moustakas, J. 2009, *Annual Review of Astronomy and Astrophysics*, 47, 159, doi: 10.1146/annurev-astro-082708-101734
- Blanton, M. R., & Roweis, S. 2007, *The Astronomical Journal*, 133, 734, doi: 10.1086/510127
- Blanton, M. R., Hogg, D. W., Bahcall, N. A., et al. 2003, *The Astrophysical Journal*, 594, 186, doi: 10.1086/375528
- Blanton, M. R., Schlegel, D. J., Strauss, M. A., et al. 2005, *The Astronomical Journal*, 129, 2562, doi: 10.1086/429803
- Borch, A., Meisenheimer, K., Bell, E. F., et al. 2006, *Astronomy and Astrophysics*, 453, 869, doi: 10.1051/0004-6361:20054376
- Brinchmann, J., Charlot, S., White, S. D. M., et al. 2004, *Monthly Notices of the Royal Astronomical Society*, 351, 1151, doi: 10.1111/j.1365-2966.2004.07881.x
- Bundy, K., Ellis, R. S., Conselice, C. J., et al. 2006, *The Astrophysical Journal*, 651, 120, doi: 10.1086/507456
- Calderon, V. F., Berlind, A. A., & Sinha, M. 2018, *Monthly Notices of the Royal Astronomical Society*, 480, 2031, doi: 10.1093/mnras/sty2000
- Cameron, E., & Pettitt, A. N. 2012, *Monthly Notices of the Royal Astronomical Society*, 425, 44, doi: 10.1111/j.1365-2966.2012.21371.x
- Campbell, D., van den Bosch, F. C., Hearin, A., et al. 2015, *Monthly Notices of the Royal Astronomical Society*, 452, 444, doi: 10.1093/mnras/stv1091
- Carnall, A. C., Leja, J., Johnson, B. D., et al. 2018, arXiv:1811.03635 [astro-ph]. <https://arxiv.org/abs/1811.03635>
- Chabrier, G. 2003, *Publications of the Astronomical Society of the Pacific*, 115, 763, doi: 10.1086/376392
- Cohn, J. D. 2017, *Monthly Notices of the Royal Astronomical Society*, 466, 2718, doi: 10.1093/mnras/stw3202
- Collaboration, D., Aghamousa, A., Aguilar, J., et al. 2016, arXiv:1611.00036 [astro-ph]. <https://arxiv.org/abs/1611.00036>
- Conroy, C., Gunn, J. E., & White, M. 2009, *The Astrophysical Journal*, 699, 486, doi: 10.1088/0004-637X/699/1/486
- Conroy, C., Wechsler, R. H., & Kravtsov, A. V. 2006, *The Astrophysical Journal*, 647, 201, doi: 10.1086/503602
- Conroy, C., Prada, F., Newman, J. A., et al. 2007, *The Astrophysical Journal*, 654, 153, doi: 10.1086/509632
- Croton, D. J., Gao, L., & White, S. D. M. 2007, *Monthly Notices of the Royal Astronomical Society*, 374, 1303, doi: 10.1111/j.1365-2966.2006.11230.x
- Croton, D. J., Stevens, A. R. H., Tonini, C., et al. 2016, *The Astrophysical Journal Supplement Series*, 222, 22, doi: 10.3847/0067-0049/222/2/22
- Daddi, E., Dickinson, M., Morrison, G., et al. 2007, *The Astrophysical Journal*, 670, 156, doi: 10.1086/521818
- Davis, M., Efstathiou, G., Frenk, C. S., & White, S. D. M. 1985, *The Astrophysical Journal*, 292, 371, doi: 10.1086/163168
- Diemer, B., Sparre, M., Abramson, L. E., & Torrey, P. 2017, *The Astrophysical Journal*, 839, 26, doi: 10.3847/1538-4357/aa68e5
- Drory, N., Bundy, K., Leauthaud, A., et al. 2009, *The Astrophysical Journal*, 707, 1595, doi: 10.1088/0004-637X/707/2/1595
- Elbaz, D., Daddi, E., Le Borgne, D., et al. 2007, *Astronomy and Astrophysics*, 468, 33, doi: 10.1051/0004-6361:20077525
- Gao, L., Springel, V., & White, S. D. M. 2005, *Monthly Notices of the Royal Astronomical Society*, 363, L66, doi: 10.1111/j.1745-3933.2005.00084.x
- Gao, L., & White, S. D. M. 2007, *Monthly Notices of the Royal Astronomical Society*, 377, L5, doi: 10.1111/j.1745-3933.2007.00292.x
- Genel, S., Vogelsberger, M., Springel, V., et al. 2014, *Monthly Notices of the Royal Astronomical Society*, 445, 175, doi: 10.1093/mnras/stu1654
- Gladders, M. D., Oemler, A., Dressler, A., et al. 2013, *The Astrophysical Journal*, 770, 64, doi: 10.1088/0004-637X/770/1/64
- Governato, F., Weisz, D., Pontzen, A., et al. 2015, *Monthly Notices of the Royal Astronomical Society*, 448, 792, doi: 10.1093/mnras/stu2720
- Gu, M., Conroy, C., & Behroozi, P. 2016, *The Astrophysical Journal*, 833, 2, doi: 10.3847/0004-637X/833/1/2
- Gunn, J. E., & Gott, III, J. R. 1972, *The Astrophysical Journal*, 176, 1, doi: 10.1086/151605

- Hahn, C., Beutler, F., Sinha, M., et al. 2018a, ArXiv e-prints, 1803, arXiv:1803.06348
- Hahn, C., Tinker, J. L., & Wetzell, A. R. 2017a, *The Astrophysical Journal*, 841, 6, doi: 10.3847/1538-4357/aa6d6b
- Hahn, C., Vakili, M., Walsh, K., et al. 2017b, *Monthly Notices of the Royal Astronomical Society*, 469, 2791, doi: 10.1093/mnras/stx894
- Hahn, C., Blanton, M. R., Moustakas, J., et al. 2015, *The Astrophysical Journal*, 806, 162, doi: 10.1088/0004-637X/806/2/162
- Hahn, C., Starkenburg, T. K., Choi, E., et al. 2018b
- Han, J., Eke, V. R., Frenk, C. S., et al. 2015, *Monthly Notices of the Royal Astronomical Society*, 446, 1356, doi: 10.1093/mnras/stu2178
- Hopkins, A. M., & Beacom, J. F. 2006, *The Astrophysical Journal*, 651, 142, doi: 10.1086/506610
- Hopkins, P. F., Kereš, D., Oñorbe, J., et al. 2014, *Monthly Notices of the Royal Astronomical Society*, 445, 581, doi: 10.1093/mnras/stu1738
- Ilbert, O., McCracken, H. J., Le Fèvre, O., et al. 2013, *Astronomy and Astrophysics*, 556, A55, doi: 10.1051/0004-6361/201321100
- Ishida, E. E. O., Vitenti, S. D. P., Penna-Lima, M., et al. 2015, *Astronomy and Computing*, 13, 1, doi: 10.1016/j.ascom.2015.09.001
- Karim, A., Schinnerer, E., Martínez-Sansigre, A., et al. 2011, *The Astrophysical Journal*, 730, 61, doi: 10.1088/0004-637X/730/2/61
- Kauffmann, G., Heckman, T. M., White, S. D. M., et al. 2003, *Monthly Notices of the Royal Astronomical Society*, 341, 54, doi: 10.1046/j.1365-8711.2003.06292.x
- Kelson, D. D. 2014, arXiv:1406.5191 [astro-ph]. <https://arxiv.org/abs/1406.5191>
- Khandai, N., Di Matteo, T., Croft, R., et al. 2015, *Monthly Notices of the Royal Astronomical Society*, 450, 1349, doi: 10.1093/mnras/stv627
- Kravtsov, A. V., Berlind, A. A., Wechsler, R. H., et al. 2004, *The Astrophysical Journal*, 609, 35, doi: 10.1086/420959
- Lacerna, I., Padilla, N., & Stasyszyn, F. 2014, *Monthly Notices of the Royal Astronomical Society*, 443, 3107, doi: 10.1093/mnras/stu1318
- Lange, J. U., van den Bosch, F. C., Zentner, A. R., Wang, K., & Villarreal, A. S. 2018, arXiv:1811.03596 [astro-ph]. <https://arxiv.org/abs/1811.03596>
- Larson, R. B., Tinsley, B. M., & Caldwell, C. N. 1980, *The Astrophysical Journal*, 237, 692, doi: 10.1086/157917
- Leauthaud, A., Tinker, J., Bundy, K., et al. 2012, *The Astrophysical Journal*, 744, 159, doi: 10.1088/0004-637X/744/2/159
- Lee, N., Sanders, D. B., Casey, C. M., et al. 2015, *The Astrophysical Journal*, 801, 80, doi: 10.1088/0004-637X/801/2/80
- Leja, J., Carnall, A. C., Johnson, B. D., Conroy, C., & Speagle, J. S. 2018, arXiv:1811.03637 [astro-ph]. <https://arxiv.org/abs/1811.03637>
- Leja, J., van Dokkum, P., & Franx, M. 2013, *The Astrophysical Journal*, 766, doi: 10.1088/0004-637X/766/1/33
- Leja, J., van Dokkum, P. G., Franx, M., & Whitaker, K. E. 2015, 798, 115, doi: 10.1088/0004-637X/798/2/115
- Li, C., & White, S. D. M. 2009, *Monthly Notices of the Royal Astronomical Society*, 398, 2177, doi: 10.1111/j.1365-2966.2009.15268.x
- Li, Y., Mo, H. J., & Gao, L. 2008, *Monthly Notices of the Royal Astronomical Society*, 389, 1419, doi: 10.1111/j.1365-2966.2008.13667.x
- Lim, S. H., Mo, H. J., Wang, H., & Yang, X. 2016, *Monthly Notices of the Royal Astronomical Society*, 455, 499, doi: 10.1093/mnras/stv2282
- Lu, Y., Wechsler, R. H., Somerville, R. S., et al. 2014, *The Astrophysical Journal*, 795, 123, doi: 10.1088/0004-637X/795/2/123
- Madau, P., & Dickinson, M. 2014, *Annual Review of Astronomy and Astrophysics*, 52, 415, doi: 10.1146/annurev-astro-081811-125615
- Magdis, G. E., Daddi, E., Béthermin, M., et al. 2012, *The Astrophysical Journal*, 760, 6, doi: 10.1088/0004-637X/760/1/6
- Mamon, G. A., Sanchis, T., Salvador-Solé, E., & Solanes, J. M. 2004, *Astronomy and Astrophysics*, 414, 445, doi: 10.1051/0004-6361:20034155
- Mandelbaum, R., Seljak, U., Kauffmann, G., Hirata, C. M., & Brinkmann, J. 2006, *Monthly Notices of the Royal Astronomical Society*, 368, 715, doi: 10.1111/j.1365-2966.2006.10156.x
- Marchesini, D., van Dokkum, P. G., Förster Schreiber, N. M., et al. 2009, *The Astrophysical Journal*, 701, 1765, doi: 10.1088/0004-637X/701/2/1765



- Matthee, J., Schaye, J., Crain, R. A., et al. 2017, *Monthly Notices of the Royal Astronomical Society*, 465, 2381, doi: 10.1093/mnras/stw2884
- Mitra, S., Davé, R., & Finlator, K. 2015, *Monthly Notices of the Royal Astronomical Society*, 452, 1184, doi: 10.1093/mnras/stv1387
- Mitra, S., Davé, R., Simha, V., & Finlator, K. 2017, *Monthly Notices of the Royal Astronomical Society*, 464, 2766, doi: 10.1093/mnras/stw2527
- Moore, B., Lake, G., & Katz, N. 1998, *The Astrophysical Journal*, 495, 139, doi: 10.1086/305264
- More, S., van den Bosch, F. C., Cacciato, M., et al. 2011, *Monthly Notices of the Royal Astronomical Society*, 410, 210, doi: 10.1111/j.1365-2966.2010.17436.x
- Moster, B. P., Naab, T., & White, S. D. M. 2013, *Monthly Notices of the Royal Astronomical Society*, 428, 3121, doi: 10.1093/mnras/sts261
- . 2017, arXiv:1705.05373 [astro-ph]. <https://arxiv.org/abs/1705.05373>
- Moustakas, J., Coil, A. L., Aird, J., et al. 2013, *The Astrophysical Journal*, 767, 50, doi: 10.1088/0004-637X/767/1/50
- Muzzin, A., Marchesini, D., Stefanon, M., et al. 2013, *The Astrophysical Journal*, 777, 18, doi: 10.1088/0004-637X/777/1/18
- Noeske, K. G., Weiner, B. J., Faber, S. M., et al. 2007, *The Astrophysical Journal Letters*, 660, L43, doi: 10.1086/517926
- Parejko, J. K., Sunayama, T., Padmanabhan, N., et al. 2013, *Monthly Notices of the Royal Astronomical Society*, 429, 98, doi: 10.1093/mnras/sts314
- Patel, S. G., Kelson, D. D., Williams, R. J., et al. 2015, *The Astrophysical Journal Letters*, 799, L17, doi: 10.1088/2041-8205/799/2/L17
- Peng, Y., Maiolino, R., & Cochrane, R. 2015, *Nature*, 521, 192, doi: 10.1038/nature14439
- Peng, Y.-j., Lilly, S. J., Kovač, K., et al. 2010, *The Astrophysical Journal*, 721, 193, doi: 10.1088/0004-637X/721/1/193
- Pillepich, A., Springel, V., Nelson, D., et al. 2018, *Monthly Notices of the Royal Astronomical Society*, 473, 4077, doi: 10.1093/mnras/stx2656
- Reddick, R. M., Wechsler, R. H., Tinker, J. L., & Behroozi, P. S. 2013, *The Astrophysical Journal*, 771, 30, doi: 10.1088/0004-637X/771/1/30
- Rodríguez-Puebla, A., Primack, J. R., Behroozi, P., & Faber, S. M. 2016, *Monthly Notices of the Royal Astronomical Society*, 455, 2592, doi: 10.1093/mnras/stv2513
- Roediger, J. C., & Courteau, S. 2015, *Monthly Notices of the Royal Astronomical Society*, 452, 3209, doi: 10.1093/mnras/stv1499
- Salim, S., Rich, R. M., Charlot, S., et al. 2007, *The Astrophysical Journal Supplement Series*, 173, 267, doi: 10.1086/519218
- Santini, P., Fontana, A., Grazian, A., et al. 2009, *Astronomy and Astrophysics*, 504, 751, doi: 10.1051/0004-6361/200811434
- Schreiber, C., Pannella, M., Elbaz, D., et al. 2015, *Astronomy and Astrophysics*, 575, A74, doi: 10.1051/0004-6361/201425017
- Silk, J., & Mamon, G. A. 2012, *Research in Astronomy and Astrophysics*, 12, 917, doi: 10.1088/1674-4527/12/8/004
- Somerville, R. S., & Davé, R. 2015, *Annual Review of Astronomy and Astrophysics*, 53, 51, doi: 10.1146/annurev-astro-082812-140951
- Somerville, R. S., Gilmore, R. C., Primack, J. R., & Domínguez, A. 2012, *Monthly Notices of the Royal Astronomical Society*, 423, 1992, doi: 10.1111/j.1365-2966.2012.20490.x
- Sparre, M., Hayward, C. C., Feldmann, R., et al. 2017, *Monthly Notices of the Royal Astronomical Society*, 466, 88, doi: 10.1093/mnras/stw3011
- Sparre, M., Hayward, C. C., Springel, V., et al. 2015, *Monthly Notices of the Royal Astronomical Society*, 447, 3548, doi: 10.1093/mnras/stu2713
- Speagle, J. S., Steinhardt, C. L., Capak, P. L., & Silverman, J. D. 2014, *The Astrophysical Journal Supplement Series*, 214, 15, doi: 10.1088/0067-0049/214/2/15
- Sunayama, T., Hearin, A. P., Padmanabhan, N., & Leauthaud, A. 2016, *Monthly Notices of the Royal Astronomical Society*, 458, 1510, doi: 10.1093/mnras/stw332
- Taghizadeh-Popp, M., Fall, S. M., White, R. L., & Szalay, A. S. 2015, *The Astrophysical Journal*, 801, 14, doi: 10.1088/0004-637X/801/1/14
- Tamura, N., Takato, N., Shimono, A., et al. 2016, in *Ground-Based and Airborne Instrumentation for Astronomy VI*, Vol. 9908, eprint: arXiv:1608.01075, 99081M

- Taylor, E. N., Franx, M., van Dokkum, P. G., et al. 2009, *The Astrophysical Journal*, 694, 1171, doi: 10.1088/0004-637X/694/2/1171
- Tinker, J., Wetzel, A., & Conroy, C. 2011, *ArXiv e-prints*, 1107, arXiv:1107.5046
- Tinker, J. L., Hahn, C., Mao, Y.-Y., & Wetzel, A. R. 2018a, *Monthly Notices of the Royal Astronomical Society*, 478, 4487, doi: 10.1093/mnras/sty1263
- Tinker, J. L., Hahn, C., Mao, Y.-Y., Wetzel, A. R., & Conroy, C. 2018b, *Monthly Notices of the Royal Astronomical Society*, 477, 935, doi: 10.1093/mnras/sty666
- Tinker, J. L., Leauthaud, A., Bundy, K., et al. 2013, *The Astrophysical Journal*, 778, 93, doi: 10.1088/0004-637X/778/2/93
- Tinker, J. L., Wetzel, A. R., Conroy, C., & Mao, Y.-Y. 2017a, *Monthly Notices of the Royal Astronomical Society*, 472, 2504, doi: 10.1093/mnras/stx2066
- Tinker, J. L., Brownstein, J. R., Guo, H., et al. 2017b, *The Astrophysical Journal*, 839, 121, doi: 10.3847/1538-4357/aa6845
- Tojeiro, R., Wilkins, S., Heavens, A. F., Panter, B., & Jimenez, R. 2009, *The Astrophysical Journal Supplement Series*, 185, 1, doi: 10.1088/0067-0049/185/1/1
- Tojeiro, R., Eardley, E., Peacock, J. A., et al. 2017, *Monthly Notices of the Royal Astronomical Society*, 470, 3720, doi: 10.1093/mnras/stx1466
- Vale, A., & Ostriker, J. P. 2006, *Monthly Notices of the Royal Astronomical Society*, 371, 1173, doi: 10.1111/j.1365-2966.2006.10605.x
- Velander, M., van Uitert, E., Hoekstra, H., et al. 2014, *Monthly Notices of the Royal Astronomical Society*, 437, 2111, doi: 10.1093/mnras/stt2013
- Vogelsberger, M., Genel, S., Springel, V., et al. 2014, *Monthly Notices of the Royal Astronomical Society*, 444, 1518, doi: 10.1093/mnras/stu1536
- Wang, L., Farrah, D., Oliver, S. J., et al. 2013, *Monthly Notices of the Royal Astronomical Society*, 431, 648, doi: 10.1093/mnras/stt190
- Wang, Y., Yang, X., Mo, H. J., et al. 2008, *The Astrophysical Journal*, 687, 919, doi: 10.1086/591836
- Wechsler, R. H., & Tinker, J. L. 2018, *ArXiv e-prints*, 1804, arXiv:1804.03097
- Wechsler, R. H., Zentner, A. R., Bullock, J. S., Kravtsov, A. V., & Allgood, B. 2006, *The Astrophysical Journal*, 652, 71, doi: 10.1086/507120
- Wetzel, A. R., Cohn, J. D., & White, M. 2009, *Monthly Notices of the Royal Astronomical Society*, 395, 1376, doi: 10.1111/j.1365-2966.2009.14424.x
- Wetzel, A. R., Cohn, J. D., White, M., Holz, D. E., & Warren, M. S. 2007, *The Astrophysical Journal*, 656, 139, doi: 10.1086/510444
- Wetzel, A. R., Tinker, J. L., & Conroy, C. 2012, *Monthly Notices of the Royal Astronomical Society*, 424, 232, doi: 10.1111/j.1365-2966.2012.21188.x
- Wetzel, A. R., Tinker, J. L., Conroy, C., & van den Bosch, F. C. 2013, *Monthly Notices of the Royal Astronomical Society*, 432, 336, doi: 10.1093/mnras/stt469
- . 2014, *Monthly Notices of the Royal Astronomical Society*, 439, 2687, doi: 10.1093/mnras/stu122
- Wetzel, A. R., & White, M. 2010, *Monthly Notices of the Royal Astronomical Society*, 403, 1072, doi: 10.1111/j.1365-2966.2009.16191.x
- Weyant, A., Schafer, C., & Wood-Vasey, W. M. 2013, *The Astrophysical Journal*, 764, 116, doi: 10.1088/0004-637X/764/2/116
- Whitaker, K. E., van Dokkum, P. G., Brammer, G., & Franx, M. 2012, *The Astrophysical Journal Letters*, 754, L29, doi: 10.1088/2041-8205/754/2/L29
- White, M. 2002, *The Astrophysical Journal Supplement Series*, 143, 241, doi: 10.1086/342752
- White, M., Cohn, J. D., & Smit, R. 2010, *Monthly Notices of the Royal Astronomical Society*, 408, 1818, doi: 10.1111/j.1365-2966.2010.17248.x
- Wilkinson, D. M., Maraston, C., Goddard, D., Thomas, D., & Parikh, T. 2017, arXiv:1711.00865 [astro-ph]. <https://arxiv.org/abs/1711.00865>
- Yang, X., Mo, H. J., & van den Bosch, F. C. 2006, *The Astrophysical Journal Letters*, 638, L55, doi: 10.1086/501069
- . 2009, *The Astrophysical Journal*, 695, 900, doi: 10.1088/0004-637X/695/2/900

- Yang, X., Mo, H. J., van den Bosch, F. C., & Jing, Y. P. 2005, *Monthly Notices of the Royal Astronomical Society*, 356, 1293, doi: 10.1111/j.1365-2966.2005.08560.x
- York, D. G., Adelman, J., Anderson, Jr., J. E., et al. 2000, *The Astronomical Journal*, 120, 1579, doi: 10.1086/301513
- Zehavi, I., Contreras, S., Padilla, N., et al. 2018, *The Astrophysical Journal*, 853, 84, doi: 10.3847/1538-4357/aaa54a
- Zehavi, I., Zheng, Z., Weinberg, D. H., et al. 2011, *The Astrophysical Journal*, 736, 59, doi: 10.1088/0004-637X/736/1/59
- Zheng, Z., Coil, A. L., & Zehavi, I. 2007, *The Astrophysical Journal*, 667, 760, doi: 10.1086/521074
- Zu, Y., & Mandelbaum, R. 2015, *Monthly Notices of the Royal Astronomical Society*, 454, 1161, doi: 10.1093/mnras/stv2062

